Natural Hazards (2026) 122:514
https://doi.org/10.1007/s11069-026-08271-x

ORIGINAL PAPER

Analysing impact of future emission scenarios on rainfall in rainfed agricultural zones in Northern Iraq using satellite data and CMIP6 models

Tuqa Khalid Abed[1] · Salah L. Zubaidi[1,2] · Yousif Almamalachy[3] · Mustafa Al-Mukhtar[4] · Mawada Abdellatif[5] · Sura Mohammed Abdulsahib[1] · Hatem Hameed Hussein[6]

Received: 10 June 2025 / Accepted: 27 May 2026 / Published online: 19 June 2026

Abstract

The impacts of climate change on future rainfall in northern Iraq at fine temporal and coarse spatial resolutions, covering all areas where rainfed agriculture is located and where large water-harvesting dams are being built, remain unclear. The study aims to investigate spatial-temporal changes in rainfall and their future projections in northern Iraq for the period 2021–2040 under two emission scenarios (i.e., SSP245 and SSP585). The LARS-WG model is calibrated using daily rainfall data from the baseline period (1985 to 2015) at 20 meteorological stations across five governorates, and is integrated with six global circulation models to project future rainfall. Python code, ArcGIS 10.8.2, and IDW were used to visualise the precipitation data. Results proved that rainfall in the southern and southwestern regions is significantly lower than in the northern and north-eastern regions. However, January to March tended to have greater rainfall than the other months from November to May, with a predominant rainfall range of 60–90 mm. These conditions are expected to persist in the future under both scenarios. Projected precipitation under the SSP245 and SSP585 scenarios for the period 2021–2040 shows distinct spatial and temporal variability across the study area. However, reductions in low-rainfall areas and increases in higher precipitation classes were evident, with some areas expected to increase by >120 mm. For instance, in March, the annual rainfall under SSP585 increased from 1.75% during 2006–2015 to 10.44% during 2031–2040. These findings introduce novel, spatially explicit insights that strengthen sustainable development planning by enabling targeted water resource management, climate adaptation strategies, and risk-informed infrastructure design under future climate scenarios.

Keywords Climate forecasting. Precipitation. Spatial and temporal analysis. SDGs. Sustainable water resources management

Extended author information available on the last page of the article

1 Introduction

According to the "Sixth Assessment Report" (AR6) of the Intergovernmental Panel on Climate Change (IPCC), greenhouse gas emissions (GHGs), mainly anthropogenic, have unequivocally caused global warming, with global surface temperatures rising by 1.1 °C over the period 2011–2020 relative to the span of 1850–1900. Global GHG emissions have continued to rise between 2010 and 2019, with unequal and ongoing contributions from unsustainable energy use, land-use change, lifestyles, and consumption patterns (Lee et al. 2023). Many regions of the world are witnessing increased manifestations of climate change, including reduced rainfall, rising temperatures, deteriorating air quality, and disruptions to atmospheric and oceanic systems. These shifts are among the most prominent factors that increase the severity and complexity of natural hazards, including floods, heatwaves, and droughts (Nile et al. 2019; Ostad-Ali-Askar et al. 2018). As such, it is of critical importance to analyse the future implications of climate change under emission scenarios for meteorological parameters (e.g., rainfall), which play a key role in sustaining water resources.

All projected emissions in IPCC reports show that climate change will worsen in the 21st century. The worldwide hydrological system will be greatly affected by rising Earth temperatures (Hinge et al. 2018). As a result of rising temperatures and rainfall fluctuations, water supply – particularly freshwater – is likely to decrease significantly in the future. Also, water resource sustainability requires careful planning and management that accounts for site-prevailing climate change assessments (Bessah et al. 2020; Ostad-Ali-Askari et al. 2019).

The Middle East's predominantly arid and semi-arid environments make it particularly vulnerable to the impacts of climate change and water scarcity (Hassan et al. 2025a, b; Namdar et al. 2021). Therefore, reviewing regional studies in the Middle East is gaining increasing importance, particularly those that assess the impacts of climate change on water resource availability and analyse related hydrological indicators and parameters. Recent studies by several researchers and academics have also confirmed the increasing frequency and intensity of extreme weather events in Syria (Mohammed and Fallah 2019), Turkey (Afshar et al. 2020), Iran (Usta et al. 2021) and (Abedi-Koupai et al. 2022), Saudi Arabia (Tarawneh and Chowdhury 2018), and Iraq (Hassan and Hashim 2020), which is directly attributed to the growing effects of global warming and changing atmospheric circulation patterns in the region.

Iraq has an arid-to-semiarid climate with limited water resources and low annual precipitation (Khairan et al. 2023; Zubaidi et al. 2023). The environmental situation in Iraq has changed significantly due to widespread scarcity of freshwater resources. Nevertheless, periodic sand and dust storms, heat waves, and flash and irregular floods that have their parallel in global climate changes are expected to only get worse over the years with the increased frequency of extreme weather events, causing wider environmental breakdown in most of Iraq (Jalal et al. 2025; Khalaf et al. 2022).

Researchers are increasingly relying on general climate models (GCMs) to study and predict current and future climate patterns by applying multiple emissions scenarios (Guo et al. 2017; Jasim and Awchi 2020; Xu and Wang 2019). Due to the coarse spatial resolution of these model networks, downscaling techniques are needed to transform global outputs into data more suitable for local and regional scales (Sayadi et al. 2019; Sha et al. 2021; Vallam and Qin 2018). Downscaling methods are generally divided into two main types: statistical downscaling and dynamic downscaling (Hassan et al. 2025a, b). Model outputs

derived from the Comparison of Paired Climate Models Project (CMIP) are among the most widely used sources in this field (Chen et al. 2022; Miralha et al. 2021; Modi et al. 2021). The Working Group on Paired Modelling (WGCM) within this project has developed its latest version, Generation 6 of CMIP (CMIP6), which incorporates a set of socioeconomic pathways (SSPs) based on different assumptions about population growth, economic patterns, and future emissions policies (Liu et al. 2023).

One of the most frequently used models for statistical downscaling and evaluating the effects of climate change is the "Long Ashton Research Station Weather Generator" (LARS-WG) model (Hassan et al. 2023; Munawar et al. 2022; Saddique 2019). This model is characterised by its low computational cost, ease of operation, and limited computing resources compared to dynamic downscaling strategies (Hernanz et al. 2021; Reder et al. 2025; Saeed et al. 2022). LARS-WG has gained widespread adoption in applied studies worldwide, having been successfully used in numerous climatic regions, including Asia (Rafiei-Sardooi et al. 2022; Saeed et al. 2021; Sharma et al. 2018), Africa (Birara et al. 2020; Kavwenje et al. 2021; Tibangayuka et al. 2022), Europe (Musayev et al. 2018; Trnka et al. 2021; Vesely et al. 2019), Australia (Shaygan et al. 2018), and North America (Alam et al. 2018, 2020; Gitau et al. 2018), reflecting its flexibility in simulating diverse climatic conditions across different geographical environments.

Climate change directly impacts the productivity of many areas in Iraq, particularly in the north, where rainfed agriculture is used to cultivate needed crops (Ahmad et al. 2021). Recent years have witnessed growing academic interest in investigating the impacts of climate change on climatic factors. For example, Dheyaa et al. (2024) conducted a study using the LARS-WG model to assess the impacts of climate change on temperature and rainfall in the cities of Baghdad, Wasit, and Maysan within the Tigris River basin (Iraq). They relied on CMIP6 models under the SSP126, SSP245, and SSP585 scenarios. Future projections indicate a gradual increase in temperatures of 1.86 to 5.36 °C by the end of the current century, and significant fluctuations in rainfall patterns across seasons, with the highest values recorded in December and January. All climate models show a consistent trend toward rising temperatures and declining rainfall patterns, suggesting potential negative impacts on water and food security in Iraq. Saeed et al. (2022) performed a study to analyse the hydrological response of the Diyala River basin, shared by Iraq and Iran, to climate change. They used a combination of statistical and hydrological models, including the LARS-WG for climate data downscaling and the SWAT hydrological model for surface runoff simulation, based on data from five GCMs within the CMIP5 project. Three emission scenarios (RCP2.6, RCP4.5, and RCP8.5) were applied to estimate changes over the future periods 2021–2040, 2041–2060, and 2061–2080. The results showed a gradual increase in temperatures of up to 16.6%, accompanied by a decrease in rainfall of up to 8.7%, leading to a decline in surface runoff exceeding 50% by the end of the century. This, in turn, reduces surface water supply during dry seasons.

Moreover, there is a growing body of regional studies that recognises the importance of evaluating the effects of climate change on temperatures and rainfall patterns in neighbouring regions, aiming to understand common climate trends in the Middle Eastern and semi-arid environments, and to determine the extent to which they are affected by future emissions scenarios. For instance, Munawar et al. (2022) conducted a study in the Jhelum River basin in the Himalayas to compare the efficiency of the Statistical Downscaling Methods (SDSM) and LARS-WG statistical reduction techniques in simulating future climate

changes using CMIP5 data. The results showed that the LARS-WG model was superior in representing rainfall variability. At the same time, SDSM was more accurate in simulating temperatures, predicting a temperature increase of 2.3–4.6 °C and an increase in rainfall of up to 11.5% in future periods. The study confirmed the importance of using statistical downscaling techniques as effective tools for estimating the impacts of climate change in complex mountain basins. Siddig et al. (2020) conducted a study analysing the impacts of climate change on agriculture in Sudan using the LARS-WG model to generate future climate data under the RCP4.5 and RCP8.5 emission scenarios for the period up to 2050. The study integrated the LARS-WG outputs with agricultural and economic models to assess the climate impacts on agricultural production. The results showed a projected increase in temperatures and fluctuations in rainfall patterns, negatively impacting rainfed agriculture and increasing the risks of drought and flooding. The study recommended the adoption of agricultural and water adaptation policies based on climate models such as LARS-WG to improve future planning in arid environments.

Based on previous studies in northern Iraq, particularly those focusing on rainfed agricultural areas, it is evident that several researchers have relied on the LARS-WG model to project future rainfall. These studies have varied between temporal analyses focused on climate variations over specific time periods (Mohammed and Scholz 2019; Muhaisen et al. 2024; Sabri and Khayyun 2024) and spatiotemporal analyses aimed at representing spatial patterns of precipitation (Al-Hasani et al. 2023; Saeed et al. 2021). Despite their importance, these studies faced several methodological limitations, most notably: (1) reliance on a limited number of weather stations spread across a narrow geographical area, which affected the accuracy of representing spatial variations in rainfall in the region, and (2) reliance on climate models from the CMIP5 project, which no longer reflect the latest updates to the sixth-generation global models (CMIP6), and therefore may limit the accuracy of climate predictions in the local context. The first study to investigate the spatial and temporal effects of climate change on all rainfed areas in northern Iraq was by Abdulsahib et al. (2024). The study provided policymakers with valuable seasonal information on managing water resources during drought or flood conditions. However, the study suffered from some limitations: (1) Using a limited number of meteorological stations. (2) Employed satellite data (NASA) with coarse resolution (0.5° × 0.625°) as observed data. (3) Employed only 5 GCMs. (4) Presented the spatiotemporal impact of climate change seasonally instead of monthly. Overall, the literature indicated that studies anticipated variable precipitation patterns and tended to show decreases in precipitation. Also, they expected rising temperatures, which led to higher evaporation rates, exacerbating the water scarcity problem. This presentation demonstrates a gradual increase in the comprehensiveness of recent studies, particularly in the geographical distribution of stations and the types of analysis used, reflecting growing scientific interest in more accurately monitoring the effects of climate change in northern Iraq. However, climate change and its consequences are an important but understudied cause for concern.

Considering all this evidence and the authors' knowledge, it seems that previous studies assessing climate change impacts on rainfall in northern Iraq have suffered from certain methodological limitations. No previous study has examined monthly spatial-temporal rainfall (quantity and distribution) sufficient to cover the total area specified for rainfed agriculture and the areas where large water-harvesting dams are located. Also, no previous study has reported monthly spatial-temporal rainfall alterations every 10 years over

approximately 50 years. Moreover, it is still uncertain whether climate change might alter seasonal timing and duration (i.e., shifts in rainfall timing).

Iraq, especially its northern regions, relies mainly on rainfall to replenish surface and groundwater sources that feed vital sectors such as agriculture and drinking water. Consequently, any change in the pattern of this rainfall due to climate change would directly threaten water and food security systems. The United Nations Water Development Report indicated that agriculture consumes about 69% of the world's available freshwater, mainly for irrigation (Pereira et al. 2023). In this context, it is clear that water use in Iraq is primarily concentrated in three sectors: agriculture, housing, and energy/industry. Agriculture, a pivotal sector in achieving national food security, accounts for approximately 85% of total water withdrawals (Marcellin et al. 2024). The continuation of traditional water management practices and agricultural techniques exacerbates water scarcity in Iraq (Adamo et al. 2018; Mueller et al. 2021; Price 2018), thereby increasing the environmental, social, and economic pressures associated with climate change.

The current research responds to the increasing environmental challenges facing the northern region of Iraq, driven by global climate change, particularly changes in rainfall patterns, which are a vital factor in the balance of water resources. This research is directly linked to the Sustainable Development Goals, particularly Goal 6 ("Clean Water and Sanitation"), which emphasises the importance of sustainable water resource management, and Goal 13 ("Climate Action"), which calls for urgent action to combat the impacts of climate change. This research contributes to supporting future environmental and water planning by providing accurate scientific predictions based on globally recognised climate models and spatio-temporal data, assisting decision-makers in developing effective adaptation policies and enhancing water security in Iraq.

This research aims to anticipate these potential changes using climate modelling tools and geographic analysis, enabling proactive measures in natural resource management and land use planning that align with global trends toward climate security and environmental sustainability. To achieve this aim, a set of objectives was identified that contribute to detailing the research steps and guiding its practical phases, as follows:

1. To calibrate and apply the LARS-WG (version 8) climate model using daily rainfall data from satellite sources (0.05° × 0.05°) for the period (1985–2010) to downscale and generate future rainfall data covering the period (2021–2040), using data from 20 meteorological stations distributed across five northern Iraqi governorates.
2. To apply projections of six GCMs of the sixth IPCC report (CMIP6) to assess the effect of two climate scenarios (SSP245 and SSP585), to get a broad range of potential future outcomes, and to diminish the uncertainty in future projections.
3. To identify monthly, spatiotemporal differences in precipitation by comparing actual and estimated values, emphasising the variability of precipitation in each of the future scenarios, and discussing the possibility of changes or variations in monthly rain patterns. This includes dividing past and future periods into 10-year intervals to improve temporal accuracy and detect subtle changes in rainfall in rainfed agricultural areas of northern Iraq.
4. To use "Geographic Information System" (GIS) and "Inverse Distance Weighting" (IDW) techniques to produce accurate spatial maps that illustrate rainfall distribution over the studied periods.

5. To provide reliable scientific data that contributes to supporting environmental and regional planning, particularly concerning water resource management, climate change adaptation, and mitigating the risks of extreme hydrological events in the short and medium term.

2 Materials and methods

2.1 Study area and dataset

Iraq is a Middle Eastern nation in Western Asia, situated between the longitudes of 38.45° and 48° east and the latitudes of 29.5° and 37.22° north. It covers a large area of about 437,072 square kilometres. The weather in the country is generally mild to cold in winter and hot and dry in summer, with temperatures rising very high on many occasions, as the average annual precipitation is lower at 166 millimetres (Ahmad et al. 2021). Also, northern Iraq is very much cooler than southern Iraq of late (Ewaid et al. 2019). The local research area is in northern Iraq and involves five mainland provinces: Duhok, Erbil, Sulaymaniyah, Mosul, and Kirkuk. The geographical area extends between latitudes 35°34′ and 37°20′ north and longitudes 41°16′ and 46°20′ east, covering an area of approximately 65,000 km². About 26% of Iraq's total area is arable (11.5 million hectares), and the entire cultivated area is around 6 million hectares, of which close 50% is in rainfed conditions in the north of the country (Ewaid et al. 2020). The climate of northern Iraq is classified as semi-arid, characterised by cold, wet winters and hot, dry summers. Maximum temperatures in July and August range from 39 to 43 °C and may locally reach 50 °C in the lowlands, while more moderate conditions prevail in the mountainous regions. In winter, maximum temperatures range from 7 to 13 °C, while minimum temperatures range from 2 to 7 °C, with the possibility of frost. The annual rainfall varies significantly, exceeding 1,000 mm in the eastern parts and falling to less than 300 mm in the western parts of the study area (Ahmad et al. 2021).

The region is strategically important for water resource management due to its presence in the tributaries of the Tigris River and several vital dams (Awchi and Kalyana 2017). Given the significant shortcomings in the availability of ground-based climate data in recent decades due to unstable security conditions and the accompanying wars and acts of terrorism, this study relied on high-resolution satellite data, particularly the Climate Hazards Group InfraRed Precipitation with Stations (CHIRPS) daily rainfall data. In a previous study (Ahmad et al. 2021) conducted in the northern region of Iraq, the CHIRPS satellite data were compared with observed data from nine meteorological stations for the period 2000–2014 to verify their accuracy and reliability. Five statistical measures were used to measure the performance of CHIRPS data in representing rainfall. The results showed that the CHIRPS rainfall is suitable for accurately represent rainfall time series in the study area because it has good relationships and relatively low CHIRPS error and bias compared to observed rainfall. Twenty meteorological stations were selected within the study area. Table S1 shows each station's geographical coordinates and elevation above sea level. The map in Fig. 1 also shows the geographical locations of these stations.

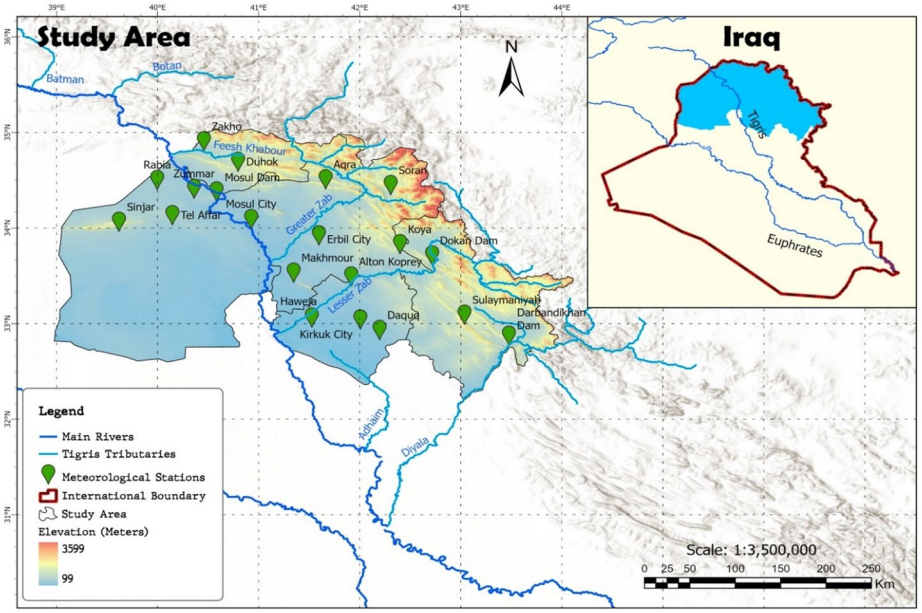

Fig. 1 The study area's selected meteorological sites and their locations

2.2 Downscaling using LARS-WG (8.0)

The LARS-WG model is a stochastic weather generator used to simulate current and project future climate conditions by generating daily time series of precipitation, minimum and maximum temperatures, and solar radiation at specified locations (Hassan et al. 2023; Mohammed and Hassan 2022). It was developed to simulate future daily time-series data to examine the impact of climate change (Mohammed and Hassan 2022). This study employs LARS-WG 8.0, which includes output information from multiple GCMs. The LARS-WG model requires entering station-specific information (name, location, elevation) and daily climate data for the base period. Once the model is configured, it is used to simulate climatic factors for the reference period (1985–2015). The model was then further applied to project future climate factors for the period 2021–2040 under two scenarios from six GCMs.

The model is assessed by examining its ability to simulate climatic factors during the baseline period using various statistical criteria and graphical tests. These tests include Brier Score, mean absolute error (MAE), correlation coefficient (R), mean bias error (MBE), root mean square error (RMSE), the Kolmogorov-Smirnov (K-S) test, and the *P* value. The K-S test was conducted to assess the equality of the distributions of daily rainfall calculated from measured and simulated data. Additionally, the *p* value was used to accept or reject the hypothesis that both datasets (measured and simulated) are likely from the same distribution. A very high *p* value and a low K-S value indicate that the simulated climate is likely similar to the measured climate, indicating that the prediction model is acceptable. Also, it is recommended to use a *p* value of 0.01 as the significance level for acceptance rather than 0.05, which is used in most statistics, to increase accuracy (Cruz-González1 et al. 2025). Table 1 shows *p* value assessment levels and various levels of fit.

Table 1 Limitations of *P* value (Cruz-González1 et al. 2025)

P value	Assessment
1	Perfect
>0.7 a 1	Very good
>0.4 a 0.7	Good
<0.4	Poor

Statistical downscaling using LARS-WG involves downscaling the GCM outputs from coarse to finer resolutions, even at a single climatic station (Lee et al. 2020). GCMs, developed by modelling groups worldwide under the CMIP, are commonly used to study the effects of past, present, and future climate changes on a global (Nguyen et al. 2024). Furthermore, CMIP6, as utilised in the present research, shows significant advantages over the previous phase (CMIP5) (Birara et al. 2020; Hamed et al. 2022). Figure 2 summarises the methods used in this investigation.

LARS-WG (8.0) was used as the model in this study, along with two climate scenarios (SSP245 and SSP585) and six CMIP6 GCMs, to downscale future precipitation (Tables S2 and S3). The model was calibrated using baseline data from 1985 to 2015 at 20 meteorological stations in the nominated study area to generate daily rainfall data for the period (2021–2040). Some research supports the concept that the model selection has little impact on the results of simulations based on climate projections (Song et al. 2020; Talukder et al. 2025), and the structural integrity of GCMs is one of the most significant sources of uncertainty in climate forecasts, as multiple studies have shown (Bilbao-Barrenetxea et al. 2024; Senatore et al. 2022; Wu et al. 2022). Therefore, fitting an ensemble average of multiple climate models can yield a better estimate of uncertainty (Azad and Ahmadi 2024). With this in mind, the use of the mean ensemble of six GCMs mitigates the influence of uncertainty stemming from the various structural characteristics of the climate models, thereby increasing the trustworthiness of future predictions in this research.

The baseline climate data used in this study consist of daily satellite-derived precipitation data obtained from CHIRPS climate products for the base period 1985–2015. Although CHIRPS climate products are originally available as gridded (pixel-based) datasets, in this study, the data were downloaded directly as point-based daily time series corresponding to the 20 selected meteorological station locations (due to the lack of data directly from these stations). Therefore, the baseline dataset used for LARS-WG calibration and validation was already in station-based format and did not require further pixel-to-point conversion. LARS-WG (version 8.0) is fundamentally a point-based stochastic weather generator that requires station-specific daily time-series input. Therefore, the model was calibrated and validated using the 20 station-based datasets. The outputs were subsequently spatially interpolated in GIS to generate continuous precipitation maps.

3 Results

3.1 Model calibration

The daily rainfall time series data (1985–2015) from CHIRPS across 20 meteorological stations were fed to the LARS-WG technique separately (i.e., station by station) to assess its capacity to simulate rainfall data over the same time span. The CHIRPS data are named

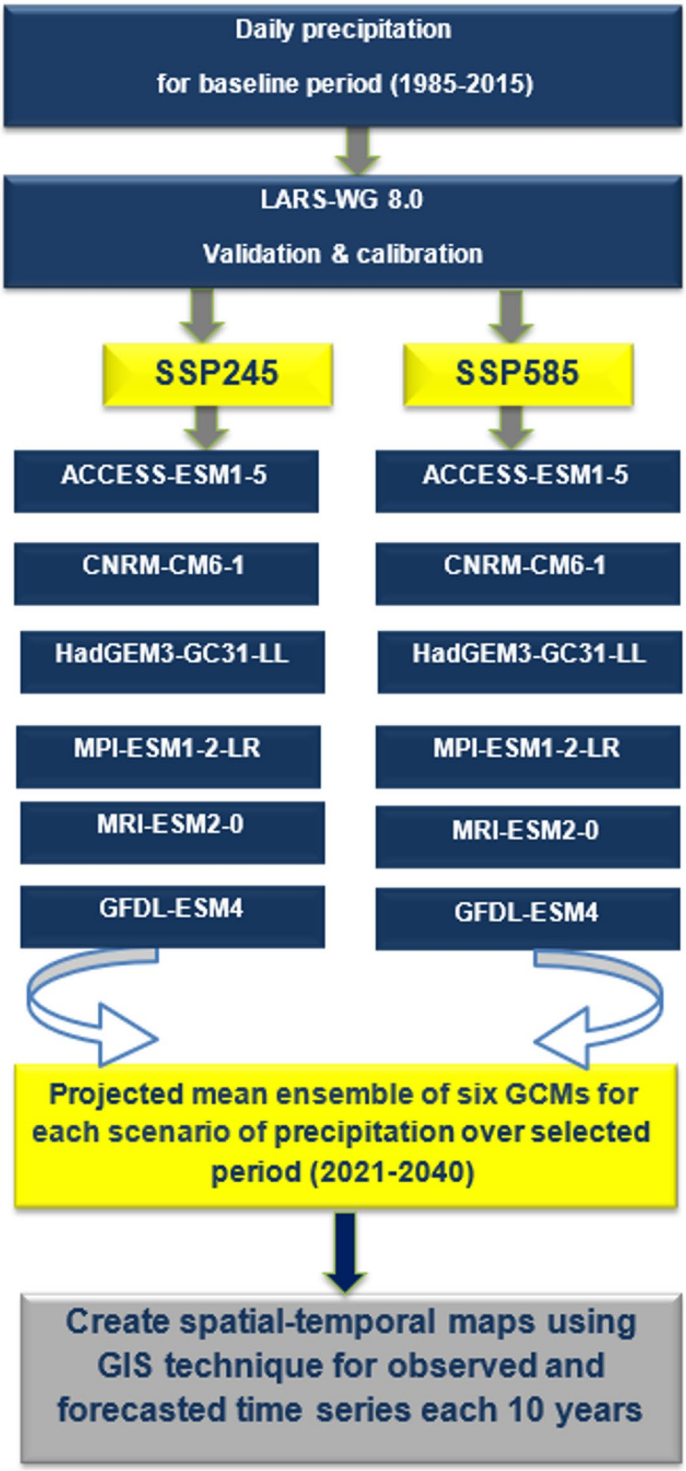

Fig. 2 Research methodological framework proposed

as actual or observed data to distinguish them from the simulated data generated during the calibration of the LARS-WG model for the same period or for subsequent comparison with future projections. To assess the LARS-WG model's capability and efficiency in simulating rainfall data during the baseline period, various statistical and graphical tests were used. Table 2 presents the outcomes of Daquq Station as an example. What stands out in the table is the LARS-WG model's ability to simulate rainfall data, ranging from very good to perfect, according to the *P* value limitations assessment in Table 1, except for months with no rainfall during the summer season.

Further statistical test analysis, including Brier Score, mean absolute error (MAE), correlation coefficient (R), mean bias error (MBE), and root mean square error (RMSE), applies to illustrate the technique's reliability in simulating rainfall data during the baseline period at Kirkuk Station (Table S4). The values of R, MSE, MAE, and MBE indicate the LARS-WG model's ability to simulate precipitation data (Munawar et al. 2022). Also, the Brier Score value (0.070) increases the reliability of the outcomes in this research. It also underscores the reliance on powerful tests commonly used to examine hydrological and climate models (Tandon et al. 2025). Closer inspection of the table shows that moderate RMSE and MAE values indicate that the LARS-WG model can reproduce the overall pattern of monthly precipitation, whilst R indicates a moderately positive association between the actual and simulated data. The small MBE value also demonstrates little bias in the model, and the Brier Score indicates good skill in predicting rainfall events. Considered together, these measures suggest that the model is reliable for simulating rainfall data during 1985–2015.

Moreover, Fig. S1 is a bar plot comparing actual and simulated monthly precipitation at Kirkuk Station over the reference period (1985–2015). The opposing columns in the figure reflect an acceptable match of the two data sets, since they show that the model simulated the actual temporal distribution of the rainfall fairly closely. The simulated values were well aligned with the actual values during the winter months (January–March), with minor deviations, whereas during the spring months (April–May), a relative drop in simulation performance was detected due to the pronounced climatic fluctuations typical of this period. The November and December months (i.e., late autumn and winter) also reveal a better match, with modelled high precipitation rates very close to the actuals. Overall, the figure indicates that the LARS-WG technique was sufficient to replicate monthly precipitation occurrences at Kirkuk Station with reasonable accuracy. Taken together, all the above results suggest an acceptable association between the observed and simulated rainfall time series during the

Table 2 K-S-test for distributions of daily rainfall

Month	K-S	*P* value	Assessment
J	0.065	1	Perfect
F	0.065	1	Perfect
M	0.13	0.984	Very good
A	0.072	1	Perfect
M	0.093	1	Perfect
J	0.348	0.096	Poor
J	No rainfall		
A	No rainfall		
S	No rainfall		
O	0.065	1	Perfect
N	0.125	0.989	Very good
D	0.065	1	Perfect

baseline period, confirming the model's effectiveness in simulating historical rainfall. The results also indicate that the model's accuracy during the baseline period supports its credibility for generating future forecasts under the SSP245 and SSP585 scenarios.

3.2 Projection results

3.2.1 Overview

The LARS-WG (8.0) has demonstrated its efficiency in simulating daily rainfall data for 1985–2015, as shown by the model calibration results (presented in Sect. 3.1). For this reason, it was utilised in the present research to project future precipitation at 20 meteorological stations based on an ensemble of 6 GCMs (ACCESS-ESM1-5, CNRM-CM6-1, HadGEM3-GC31-LL, MPI-ESM1-2-LR, MRI-ESM2-0, and GFDL-ESM4) alongside two SSP scenarios over the period 2021–2040.

Rainfall data for each year were converted from daily to cumulative monthly values to facilitate analysis of climate patterns and determine whether there is a significant shift in rainfall behaviour during the period (2021–2040). This conversion enables the detection of seasonal trends and temporal variations in precipitation rates, helping assess the impact of climate change on water resources and plan future adaptation strategies in the region. Accordingly, the observed and projected data (i.e., from SSPs) are separated into monthly scales and focus on months from November to May. At this phase, monthly data were generated for each year across the whole period. By computing the mean precipitation for each month throughout all years for specific intervals, each nominated location was provided with 7 values for mean precipitation. These values characterise the monthly precipitation differences at each location.

The historical precipitation data series (1985–2015) was divided into three intervals: the first spanned 11 years (1985–1995), and the subsequent two intervals spanned two decades (1996–2005 and 2006–2015). Climatic modelling of future data: both scenarios (SSP245 and SSP585) have been divided into two scenario-specific 10-year periods (2021–2030 and 2031–2040). This fine-grained division is intended to further explore climate variations in precipitation behaviour, since under the mid- to long-term averages, less conspicuous climatic variations or changes that could be of interest to the environment or planning can be lost. This approach enables analysis of decadal-scale climate trends, which is one component of a more comprehensive understanding of the nature of climate change and its impact on hydrological regimes in the region. Besides, the average of the six GCMs was also computed to have a decent forecast on what the future holds (Abdulsahib et al. 2024).

To illustrate this, Fig. S2 compares monthly precipitation averages at Kirkuk Station across two GHG emission scenarios (SSP245 and SSP585) for 2031–2040. The precipitation time distribution, as shown in the figure, follows the traditional pattern of the region: the highest amounts are received in winter and early spring (December–April), and close to zero in summer (June–September). The difference between the two cases is evident in the months when SSP245 registers a comparatively higher rate: November and December, whereas the values were nearly equal in the other months, including January, March, and April. This means that the estimated high-emission scenario (SSP585) in this decade does not significantly change the total precipitation pattern compared to the moderate scenario (SSP245). Nonetheless, it can lead to a slight reduction of precipitation during certain

autumn months and a moderate rise in March. The figure shows that differences between the two scenarios gradually emerge in the medium term. At the same time, the overall rainfall distribution remains unchanged, consistent with the cumulative nature of climate change impacts in the area.

Python code, ArcGIS 10.8.2, and IDW were used to visualise the precipitation for historical and future (i.e., under both SSPs) data. The IDW method provides a fair representation of the station's variability. All actual and projected data across the study area were spatially interpolated using the IDW and mapped into classes (Awchi and Kalyana 2017; Sheikhbabaei et al. 2022) that depended on the cartographic expert knowledge of the research team and earlier research (Alasow et al. 2024; Merabti et al. 2018; Muhire et al. 2018). The following factors were also considered when selecting classes for the rainfall maps: classifications must be based on precipitation values, from lowest to highest, so that colour themes are consistent across all maps and readers can visually compare them.

1. At least seven colour classes were adopted to enhance the accuracy of the visual representation, as reducing the number of classes may result in the loss of fine spatial details of the precipitation distribution.
2. The study focused on seven distinct classifications with readily distinguishable colours to avoid confusion.
3. The classifications ranged from 0 to 210 mm, with a fixed interval of 30 mm between each category.

In conclusion, 21 figures were prepared to illustrate the temporal and spatial distribution of monthly rainfall in the study area. Each month has 7 sub-figures: the baseline period has 3 sub-figures, each representing 1 interval, and 2 sub-figures for SSP245 and SSP585, each representing 1 interval.

3.2.2 Spatiotemporal distribution maps for projection of rainfall

This section analyses spatial and temporal distribution maps of rainfall in the northern region of Iraq for historical and projected future periods, based on two climate scenarios: SSP245 and SSP585. Each month (November to May) is represented by 7 maps that show the temporal and spatial patterns of rainfall. The baseline period (1985–2015), spanning 31 years, is divided into three consecutive time intervals: the first, from 1985 to 1995 (11 years), and the second and third, each covering 10 years. Two maps are allocated to each climate scenario for future intervals (i.e., 2021–2030 and 2031–2040), representing the expected rainfall projections.

The temporal and spatial distribution maps of rainfall in November for the observed and predicted periods under two climate scenarios are shown in Figs. 3, 4 and 5. Figure 3 displays the observed period in three intervals. The first baseline interval (1985–1995) shows the dominance of two main rainfall classes: 30–60 mm and 60–90 mm. The highest rainfall rates were recorded in the northern and northeastern regions, where 11.8% of the regions fell into the 90–120 mm class, and 1.5% fell into the 120–150 mm class. During the second interval (1996–2005), the percentage of areas classified as 30–60 mm increased, while the 60–90 mm class decreased and spread across several stations, covering approximately 15.41% of the study area.

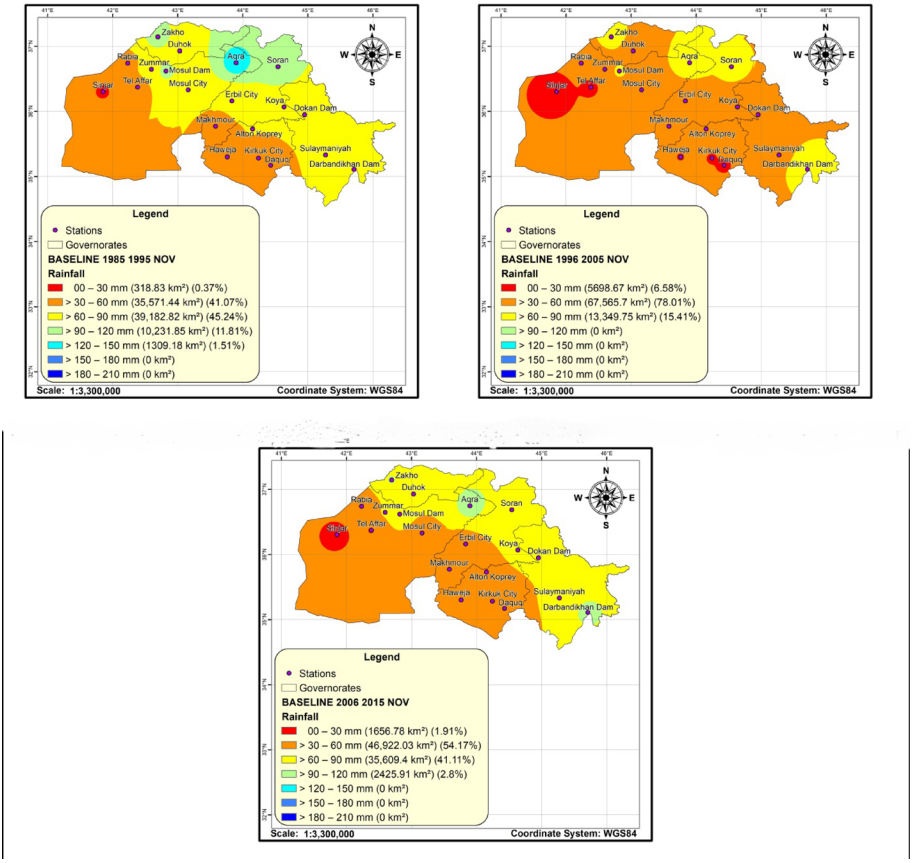

Fig. 3 Results for precipitation in November for baseline period (1985-2015)

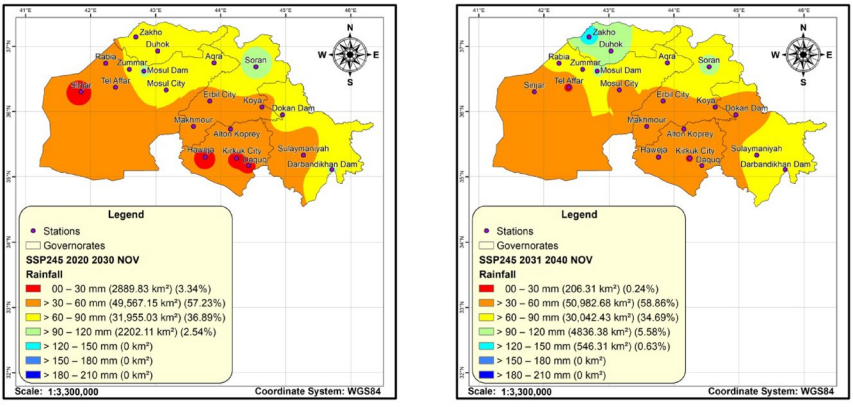

Fig. 4 Results of precipitation in November under SSP245 (2021–2040)

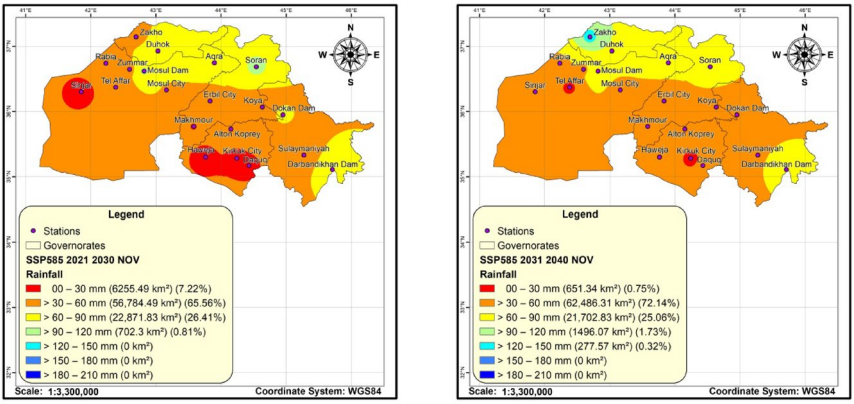

Fig. 5 Results for precipitation in November under SSP585 (2021–2040)

In contrast, areas experiencing rainfall scarcity expanded, with the percentage below 30 mm increasing from 0.37% in the first interval to 6.58% in the second interval, indicating a relative decline in rainfall in some southern and western areas. During the third interval (2006–2015), the study area witnessed a clear improvement in rainfall amounts, particularly in the northern and eastern parts, where the 60–90 mm percentage increased significantly compared to the previous interval. High rainfall was also recorded at the Aqra and Darbandikhan Dam Stations, which were classified as 90–120 mm. As shown in the maps, the mountainous areas in the northeast of the study area received the most rainfall during the baseline intervals, reflecting the significant role of topography in directing and distributing rainfall in the region. A closer inspection of the figure shows that rainfall data declined when moving from the 1st to the 3rd interval, across both rainfall class and coverage area.

For the projected rainfall data, under the SSP245 scenario (Fig. 4), maps generally expected to show that the 30–60 mm and 60–90 mm classes were the most prevalent during the intervals (2021–2030) and (2031–2040). During the first interval, limited areas of scarcity were likely observed, classified as 0–30 mm, particularly in the southern and western parts of the study area. In contrast, some other areas experienced increased precipitation, particularly in the northwest of the region, where some areas classified as 90–120 mm appeared, but they remained limited in size. During the interval (2031–2040), areas of medium and high precipitation were predicted to expand in the north, and Zakho Station was observed in the 120–150 mm class, a marked shift compared to the baseline period, when this class was often associated with Aqra Station. This shift is likely due to changes in regional wind patterns or local topographic factors that contributed to the northwestward orientation of the wet masses. The general pattern of precipitation distribution in this scenario is also evidently concentrated in the northern regions, while the southern regions remain under climatic pressure and relative dryness. This geographical variation indicates the need for localised water resource management strategies. The most interesting aspect of this figure is that, in general, both intervals are expected to show the same distribution of rainfall classes, except for some stations. Generally, the figure highlights that future rainfall data is likely to decline relative to the 3rd interval of the reference period, and the 1st interval will have a greater influence than the 2nd .

For the projected rainfall data, under the SSP585 scenario (Fig. 5), maps for the period (2021–2040) show that the dominant class in terms of precipitation amount was 30–60 mm, reflecting a moderate precipitation pattern that continued during the intervals 2021–2030 and 2031–2040. A relative improvement in rainfall distribution is observed during the second category of this phase, as the percentage of areas classified in this class increased, indicating a trend toward stabilisation of the moderate precipitation pattern at several study stations. The maps also showed a decline in the 0–30 mm class, especially in the southern regions, indicating a shrinkage of arid and semi-arid areas during this interval. On the other hand, the 90–120 mm class doubled its area during the second interval, with the emergence of limited areas classified as 120–150 mm, representing approximately 0.32% of the total study area. This may indicate an increased likelihood of heavy rainfall or localised flooding at Zakho Station. What is interesting about the rainfall classes in all the above figures for November is that the high class is distributed in the north and northeast in the past and is likely to remain the same in the future under both SSPs. Totally, the figure shows that the effect of climate change on future rainfall data is similar to that of the 1st and 2nd intervals under SSP245. The 1st interval (SSP585) differs from the others in terms of expected future rainfall reductions. It is the most impactful interval, followed by the 1st (SSP245), 2nd (SSP585), and 2nd (SSP245).

Figures 6, 7 and 8 illustrates the spatial-temporal distribution maps of rainfall in December for the observed and predicted periods under two climate scenarios. Figure 6 reveals that the most common rainfall classes during the baseline period were 60–90 mm and 90–120 mm, which cover areas ranging from about 83% to 97% of the total area. Also, in December, the study area received more rainfall than in November for the baseline period. The first interval (1985–1995) showed that most of the study areas received rainfall in the 60–90 mm class, followed by 90–120 mm (26.74%), while only 3.26% received rainfall in the 30–60 mm class. What is clearly seen in this figure is the high rainfall class (90–120 mm) located in the northeast of the study area. The map for the second interval (1996–2005) revealed areas with high rainfall of 120–150 mm, covering 7.27% of the study area, while the prevalent class remained 60–90 mm. Also, this interval differs from the previous one in the 90–120 mm class, which is separated in the north more than in the northeast. During the third interval of the baseline period (2006–2015), a general decline in rainfall was observed, with areas recording less than 90 mm becoming more prevalent (i.e.,>93%), while areas with high rainfall rates declined significantly. The maps show that areas with high rates exhibit a significant decline, especially in the region's northeast.

The future rainfall data under the SSP245 scenario (Fig. 7) expect higher rainfall amounts than during the third interval of the baseline period, and the 2nd interval will likely witness rainfall amounts greater than the 1st. During the interval (2021–2030), the percentage of areas classified as 60–90 mm is likely to increase from 76.51% to 86.04%. Rainfall in the 90–120 mm class is expected to be concentrated at the Zakho, Sulaymaniyah, Mosul Dam, and Duhok Stations. At the same time, the 60–90 mm class is likely to be concentrated at the Alton Koprey, Haweja, and Makhmour Stations. During the second interval (2031–2040), the region is forecast to experience a further increase in rainfall compared with the 1st interval, especially in the 90–120 mm class, which is expected to increase from 6.73% to 39.36%. Rainfall in the 120–150 class is also likely to occur at some stations (e.g., Soran and Darbandikhan Dam Stations), covering 5.02% of the study area. The maps show that high rainfall is predicted to be concentrated in the mountainous regions to the north and

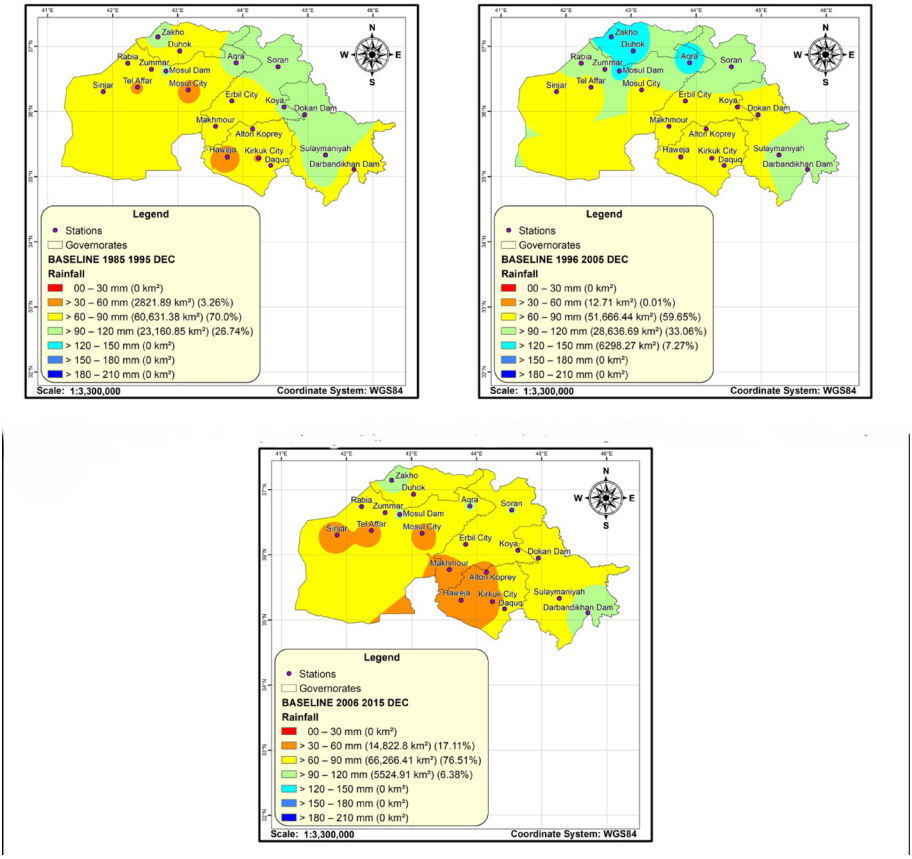

Fig. 6 Results for precipitation in December for baseline period (1985-2015)

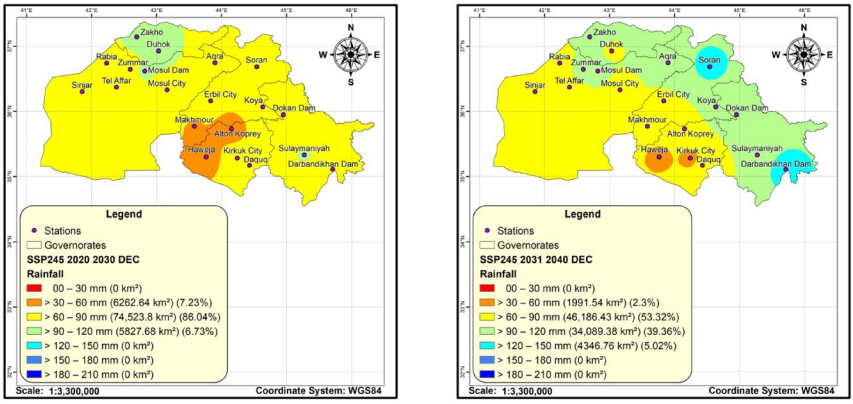

Fig. 7 Results of precipitation in December under SSP245 for (2021–2040)

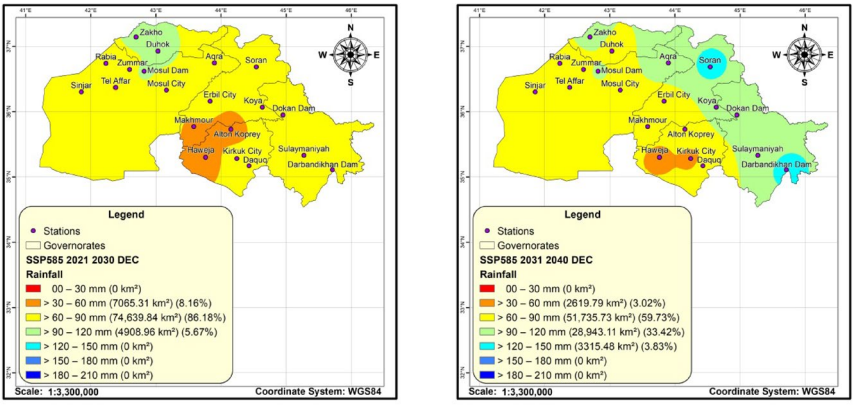

Fig. 8 Results for precipitation in December under SSP585 for (2021–2040)

northeast of the study area, particularly at the Soran and Darbandikhan Dam Stations, which have moved into the 120–150 mm class.

For the projected rainfall data under the SSP585 scenario spans (2021–2040) (Fig. 8), it is forecast to receive more rainfall than the 3rd interval of the historical period. The 1st interval of both SSPs is likely to share the pattern of rainfall classes, and it is expected that the same thing will happen for the 2nd interval for both SSPs. However, the 2nd interval (SSP245) is projected to receive the highest rainfall amounts, followed by the 2nd (SSP585), the 1st (SSP245), and the 1st (SSP585). Maps for the interval (2021–2030) show that the dominant rainfall class is expected to receive 60–90 mm, accounting for 86.81% of the total area. At the same time, the Zakho, Duhok, and Mosul Dam Stations are predicted to receive 90–120 mm class. In contrast, rainfall amounts are expected to be the lowest in Makhmour, Alton Koprey, and Haweja, at 30–60 mm class. During the second interval (2031–2040), the map is likely to show a significant increase in the area classified as 90–120 mm, rising from 5.67% to 33.42%. The highest rainfall class during this period was 120–150 mm, covering 3.83% of the total study area. Meanwhile, Haweja and Kirkuk Stations recorded the lowest rainfall amounts during this interval.

Figures 9, 10 and 11 illustrate maps prepared for the observational and predicted periods under two climate scenarios to analyse temporal and spatial rainfall variations during January. Generally, the figures show marked variation in rainfall magnitude and distribution across the three intervals of the reference phase, reflecting spatial and temporal changes in rainfall patterns. For Fig. 9, during the first interval (1985–1995), the 60–90 mm class dominated most of the study area, covering approximately 68.12%, followed by the 90–120 mm class, accounting for 19.66%. Then class 30–60 mm (9.72%), and class 120–150 mm (2.5%). The lower rainfall class tends to be concentrated in the south, whereas the higher rainfall class tends to be located in the north. During the second interval (1996–2005), rainfall exceeding 90 mm accounted for about 60% of the total area, located generally in the north and northeast. The class 180–210 mm is located at the Aqra and Zakho Stations, while the class 30–60 mm is located at the Haweja and Kirkuk City Stations. During the 3rd interval (2006–2015), the rainfall class pattern was similar to that of the 2nd interval, but rainfall amounts were generally lower. The percentage of the (60–90 mm) class increased

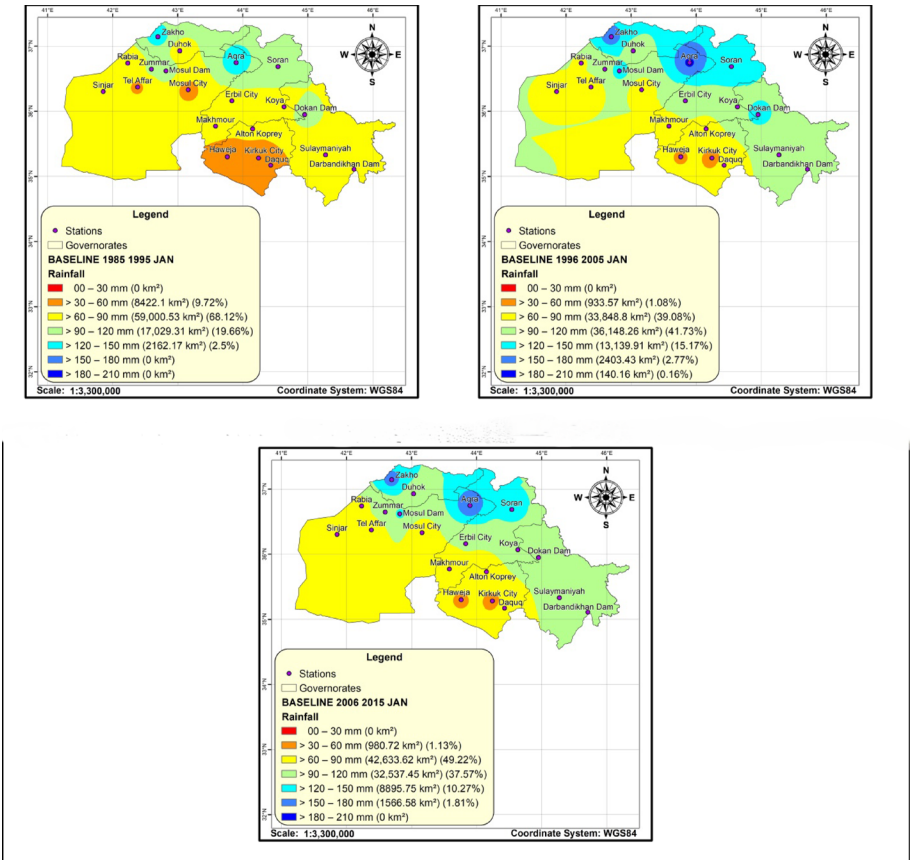

Fig. 9 Results for precipitation in January for baseline period (1985-2005)

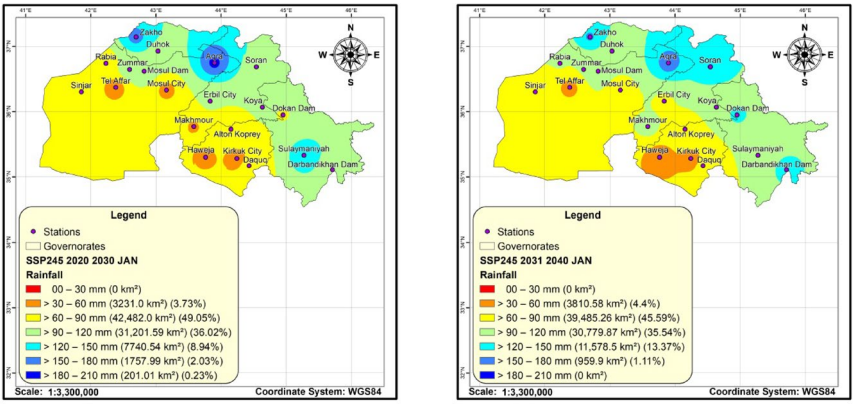

Fig. 10 Results for precipitation in January under SSP245 (2021–2040)

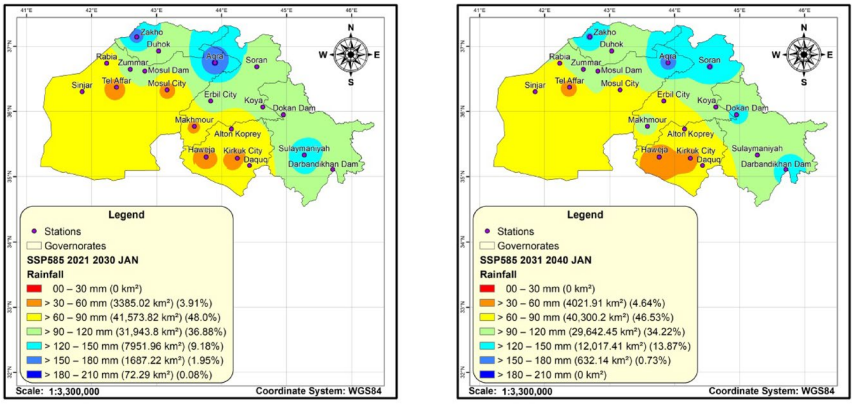

Fig. 11 Results for precipitation in January under SSP585 (2021–2040)

again (49.22%), while the (90–120 mm) class declined (37.57%), indicating fluctuations and instability in the precipitation pattern.

For the projected rainfall data under the SSP245 climate scenario (Fig. 10), both intervals (2021–2030 and 2031–2040) are likely to have the same distributions of rainfall classes across the study area. It is anticipated that the high class will be distributed to the north and northeast, while the low class will appear in limited areas in the south and southwest. For the period 2021–2030, the results will probably show that more than 49% of the study stations fall into the 60–90 mm rainfall class, followed by the 90–120 mm class, which covers 36.02% of the study area. The Zakho and Aqra Stations recorded the highest rainfall rates, falling within the 180–210 mm class, increasing the likelihood that these areas will be exposed to flooding in the future. During the second interval (2031–2040), the same rainfall classes will continue to dominate, with a noticeable shift in the classification of the Makhmour Station from the 30–60 mm class in the previous interval to the 90–120 mm class. Similarly, Dokan Dam Station will shift from the 60–90 mm class in the previous interval to the 120–150 mm class, reflecting a clear potential shift in rainfall distribution toward higher magnitudes. These changes indicate a gradual transition in some areas from light to medium precipitation, reflecting a potential future dynamic in rainfall distribution under this scenario. Generally, the figure highlights that future rainfall data is likely to decline relative to the 3rd interval of the reference period, and the 1st interval will have a greater influence than the 2nd .

For the projected rainfall data under the SSP585 scenario (Fig. 11), both intervals (2021–2030 and 2031–2040) are likely to have the same distributions of rainfall classes across the study area. It is anticipated that the high class will be distributed to the north and northeast, while the low class will appear in limited areas in the south and southwest. Also, the 1st interval of both SSPs is similar, but the SSP585 will tend to receive more rainfall. In the same vein, the 2nd interval will reveal the same rainfall pattern, but the SSP585 will tend to receive less rainfall. The mapped data for the first interval (2021–2030) is anticipated to show that the maximum rainfall class recorded was (180–210 mm) in a very limited area, while the minimum class was (30–60 mm). The highest rainfall rates will be concentrated in the north and northeastern regions of the study area. At the same time, the lowest occurred

in the south and southwestern parts, reflecting a clear spatial variation in rainfall distribution. In the second interval (2031–2040), the 60–90 mm class will remain the dominant category, covering 45.59% of the study area and concentrated in the southwestern parts. In contrast, higher classes exceeding 90 mm will be distributed in the northern and eastern regions, indicating a continued upward trend in precipitation in those areas. It is worth noting that a remarkable shift is recorded at Makhmour Station, which will move from the 30–60 mm class in the 1st interval to the 90–120 mm class in the 2nd interval, reflecting a tangible change in the local rainfall pattern in that region. Totally, the figure shows that the effect of climate change on future rainfall data is similar to that of the 1st and 2nd intervals under SSP245. The 1st interval (SSP585) differs from the others in terms of expected future rainfall reductions. It is the most impactful interval, followed by the 1st (SSP245), 2nd (SSP585), and 2nd (SSP245).

Figures 12, 13 and 14 reveal maps prepared for the observational and predicted periods under two climate scenarios to analyse spatial-temporal rainfall variations during February. Generally, the figures show marked variation in rainfall magnitude and distribution across the three intervals of the reference phase, reflecting spatial and temporal changes in rainfall patterns. In this period, the north and northeast regions received more rainfall than the

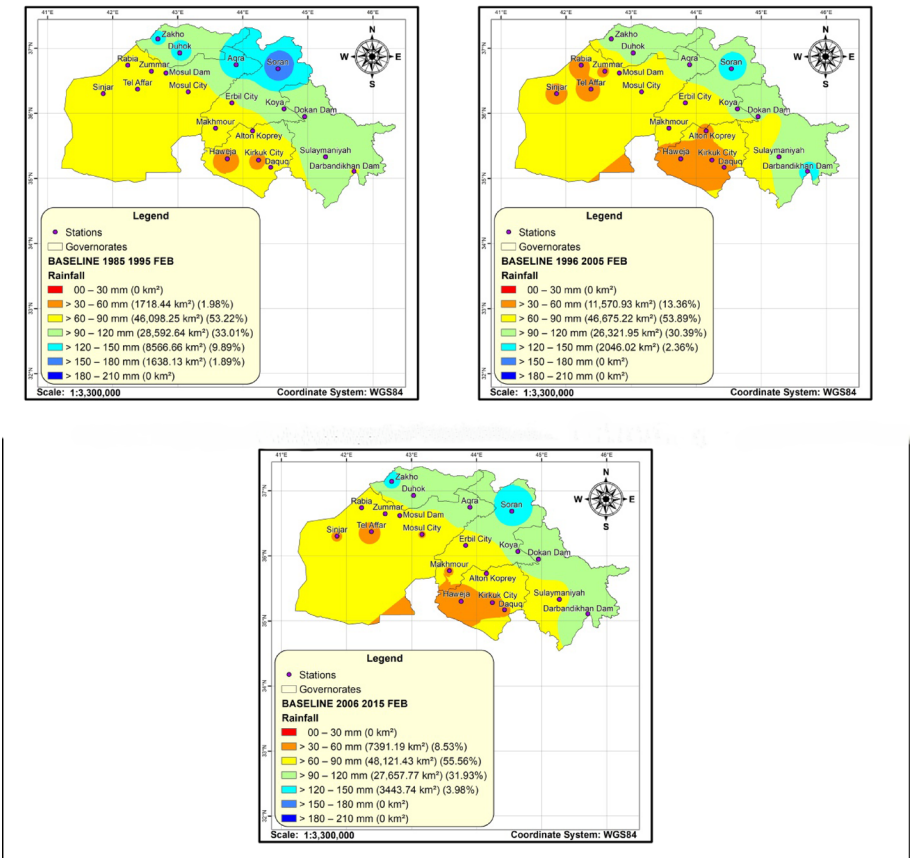

Fig. 12 Results for precipitation in February for baseline period (1985-2015)

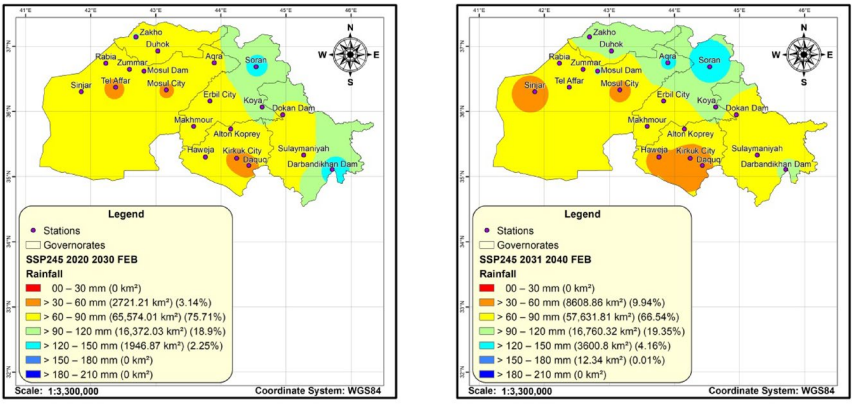

Fig. 13 Results for precipitation in February under SSP245 (2021–2040)

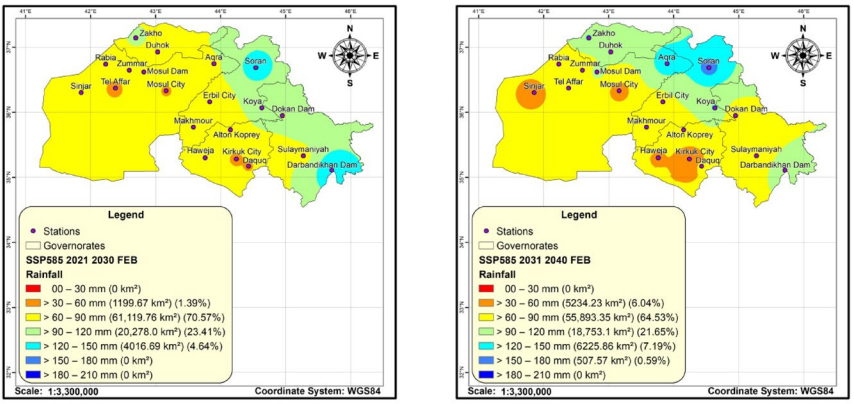

Fig. 14 Results for precipitation in February under SSP585 (2021–2040)

other regions. In contrast, the lower rainfall class was observed in limited zones in the central south and western regions. Figure 12 shows the rainfall maps for the reference period. The first map, for the interval from 1985 to 1995, indicates that the majority of the region (53.22%) received rainfall within the (60–90 mm) class, followed by the (90–120 mm) class at 33.01%. Limited areas also received larger amounts of rainfall within the (120–150 mm) and (150–180 mm) classes, at 9.89% and 1.89%, respectively. During the second interval (1996–2005), the (60–90 mm) class still accounted for the largest proportion of the area (53.89%), while the (90–120 mm) class accounted for approximately 30.39%, especially in the northeastern regions. It is worth noting that the 120–150 mm class decreased significantly by 7.53% compared to the previous interval, while the 30–60 mm class increased in the western and southern regions of Iraq. In the third interval (2006–2015), the 60–90 mm class maintained its dominance over more than half of the area, while the 120–150 mm class was concentrated in the Soran and Zakho Stations at 3.98%. Overall, the southwestern regions had the lowest rainfall rates. The most interesting aspect of this figure is that Soran

Station received the highest rainfall amount over the three intervals compared to the other stations on each map.

Figure 13 shows the projected rainfall data under the SSP245 scenario, during the period (2021–2040). Both intervals (2021–2030 and 2031–2040) will probably reveal the patterns for the 3rd interval of the baseline period, but with several shifts in limit stations. Additionally, maps for the future period are expected to show a decline in rainfall for both intervals in comparison to the 3rd reference period. The 60–90 mm class will have the highest proportion (75.71%) of the study area for the first intervals (2021–2030), followed by the 90–120 mm class at 18.9%. The 120–150 mm class will have the lowest proportion of the study area at only 2.25%. During the second interval (2031–2040), the rainfall distribution will be changed significantly, the 60–90 mm class rate dropped from (75.71%) to (66.54%). In contrast, the 90–120 mm class is expected to increase slightly to 19.35%. A significant increase will also be observed in the 30–60 mm class, rising from 3.14% to 9.94%. Generally, the figure highlights that future rainfall data is likely to decline relative to the 3rd interval of the reference period, and the 2nd interval will have a greater influence than the 1st .

According to the SSP585 scenario (Fig. 14), during the period (2021–2040), overall, the 1st interval of both SSPs is likely to share the same pattern of rainfall classes. It is expected that the same will occur for the 2nd interval for both SSPs, but the area with SSP585 is likely to receive more rainfall than in the SSP245 scenario. For the 1st interval, approximately 70.57% of the study area is anticipated to be covered by the 60–90 mm class, followed by the 90–120 mm class at 23.41%. During this interval, no areas were recorded falling into the classes below 30 mm or above 150 mm, indicating relative stability in rainfall limits. In the second interval (2031–2040), the 60–90 mm class is likely to maintain its predominance at 64.53%, while the 150–180 mm class will be recorded at 0.59%, a level not observed in the previous interval. Aqra Station will also witness a shift from the 60–90 mm class to the 120–150 mm class, indicating a localised increase in rainfall. The 1st interval will differ from the 2nd interval of SSP585 in the distribution of high-class rainfall. For the 1st interval, the high classes will be located in the east, while for the 2nd interval, they will be located in the north. Totally, the figure shows that the effect of climate change on future rainfall data is similar to that of the 1st and 2nd intervals under SSP245. The 2nd interval (SSP245) differs from the others in terms of expected future rainfall reductions. It is the most impactful interval, followed by the 2nd (SSP585), 1st (SSP245), and 1st interval (SSP585).

Figures 15, 16 and 17 reveal maps prepared for the observational and predicted periods under two climate scenarios to analyse spatial-temporal rainfall variations during March. Figure 15 shows the temporal and spatial maps of rainfall during the reference period (1985–2015). The rainfall distribution in March is generally similar to that in February over the reference period, but the study area received more rainfall in March than in February. For instance, the 90–120 mm class ranged from 30.39% to 33.01% in February and 39.48%–51.67% in March. However, the baseline period was divided into three consecutive time intervals. During the first interval (1985–1995), the data indicate that 49.08% of the studied area received rainfall within the 60–90 mm class, followed by the 90–120 mm class at 41.45%. The class (120–150 mm) were recorded at the Aqra, Soran, and Mosul Dam Stations at 7.93%, while the Sinjar Station recorded the lowest rainfall (30–60 mm) at 1.43%. In the second interval (1996–2005), the 90–120 mm class became dominant, with a coverage rate exceeding 50%, followed by the 60–90 mm class at 31.87%. The 120–150 mm class saw an increase to 16.25%. The class 150–180 mm appeared in a limited area covering the

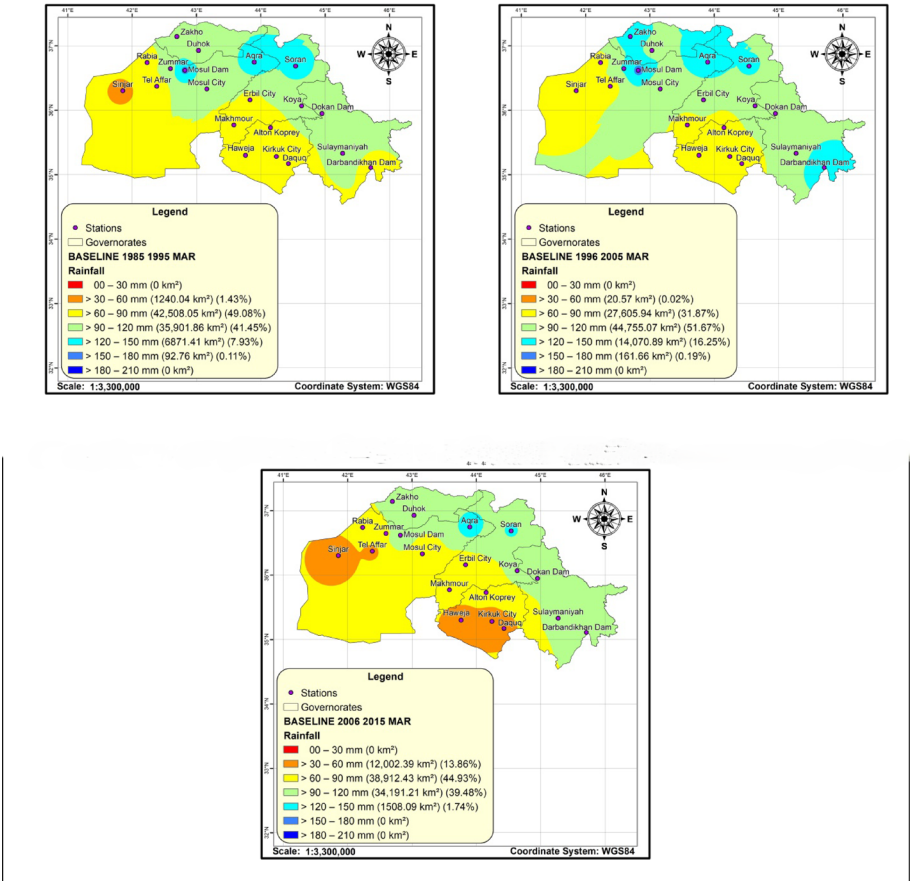

Fig. 15 Results of precipitation in March for baseline period (1985-2015)

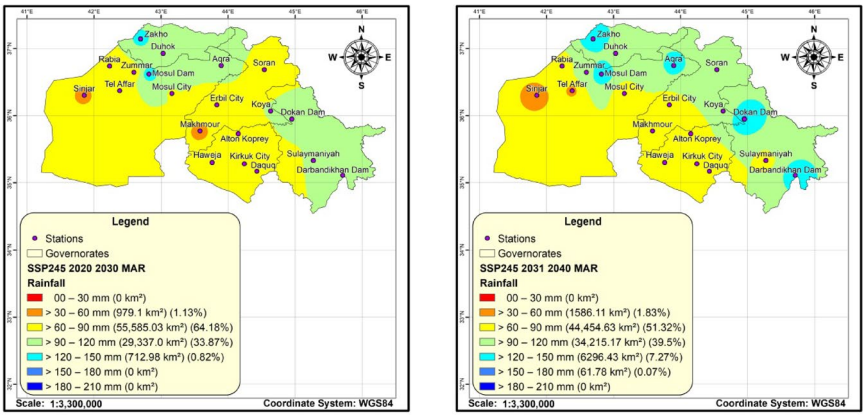

Fig. 16 Results for precipitation in March under SSP245 (2021–2040)

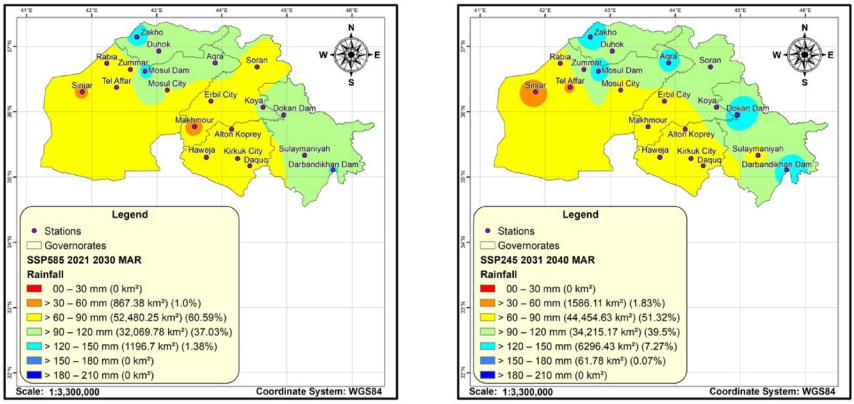

Fig. 17 Results for precipitation in March under SSP585 (2021–2040)

Mosul Dam Station. What is interesting about the data in this map is that this is the first time that the 90–120 mm class extended from the north to the south of the Mosul Area. In the 3rd interval (2006–2015), the 90–120 mm class declined to 39.48%, while the 60–90 mm class increased to 44.93%. The 30–60 mm class was recorded at approximately 13.86% of the study area, while the 120–150 mm class was limited to only the Aqra and Soran Stations.

Figure 16 shows the projected rainfall data under the SSP245 moderate climate scenario of the period (2021–2040). The map for the 1st interval (2021–2030) is likely to reveal rainfall distributions that differ from those for the 3rd interval of the baseline period in several respects. The class 90–120 mm is anticipated to decline from 41.22% in the past to the 34.69% in the future. Also, the distribution of this class in the past was from the north to the northeast, while in the future it is expected to be distributed separately in the north and east. The map will show that the most prevalent class was 60–90 mm, accounting for 64.18% of the area, followed by 90–120 mm, accounting for 33.87%. The highest rainfall amounts (120–150 mm) will be recorded at the Zakho and Mosul Dam Stations, while the lowest (30–60 mm) will be recorded at the Sinjar and Makhmour Stations, reflecting a clear spatial variation in rainfall distribution. In the 2nd interval (2031–2040), the map for the 1st interval (2021–2030) is likely to reveal rainfall distributions that are similar to those for the 3rd interval of the baseline period. For example, the class 90–120 mm is anticipated to have the same distribution and amount in the future as in the same class in the 3rd interval of historical data. Additionally, the 2nd interval will show an increase in rainfall amount compared to the 1st interval, as indicated by classes exceeding 90 mm. For instance, the 90–120 mm and 120–150 mm classes will increase from 33.87% to 39.5 and 0.82% to 7.27%, respectively.

Under the SSP585 extreme climate scenario for the period (2021–2040), the 1st interval of both SSPs is likely to exhibit the same rainfall-class pattern. It is expected that the same will occur for the 2nd interval for both SSPs, but the area with SSP585 is likely to receive more rainfall than in the SSP245 scenario. Map for the first interval (2021–2030) will show that the largest proportion of precipitation was recorded in the northern and eastern regions of the study area, specifically in the Zakho, Mosul Dam, and Darbandikhan Dam Stations, within the class (120–150 mm), but with a limited coverage of 1.38% (Fig. 17). However, the dominant class in this interval is likely (60–90 mm), with a coverage rate of 60.59%, followed by (90–120 mm), with 37.03%. Sinjar and Makhmour Stations will record the lowest

precipitation amounts within the (30–60 mm) class. In the second interval (2031–2040), the (60–90 mm) class is expected to dominate most parts of the region, especially in the southwestern parts. Meanwhile, the northeastern regions are anticipated to receive the largest amounts of rainfall within the (90–120 mm) class (36.92%). The upper class (120–150 mm) will also experience a significant expansion of 10.2%, up from 1.38% in the previous interval, and will be distributed across several stations in the north and northeast. A shift from the 30–60 mm class range at the Makhmour Station in the previous interval to the Tel Affar Station in this interval is projected, reflecting a spatial shift in the arid zones.

Maps prepared for the observational and predicted periods under two climate scenarios to analyse spatial-temporal rainfall variations during April are presented in Figs. 18, 19 and 20. During the reference period (1985–2015), divided into three consecutive time intervals, the rainfall maps showed clear variation in both spatial and temporal distributions (Fig. 18). Rainfall amounts declined compared with the baseline period in March. Additionally, the 60–90 mm class was dominant; the 90–120 mm class was observed in limited areas in the north, while the 30–60 mm class was distributed in the south and west. In the first interval (1985–1995), areas receiving precipitation rates between 60 and 90 mm constituted the largest proportion of the study area, accounting for 64.22%, followed by the 30–60 mm class, which accounted for 27.13%. Meanwhile, the proportion of areas receiving rainfall of 90–120 mm did not exceed 8.66%, and these areas were mainly concentrated in moun-

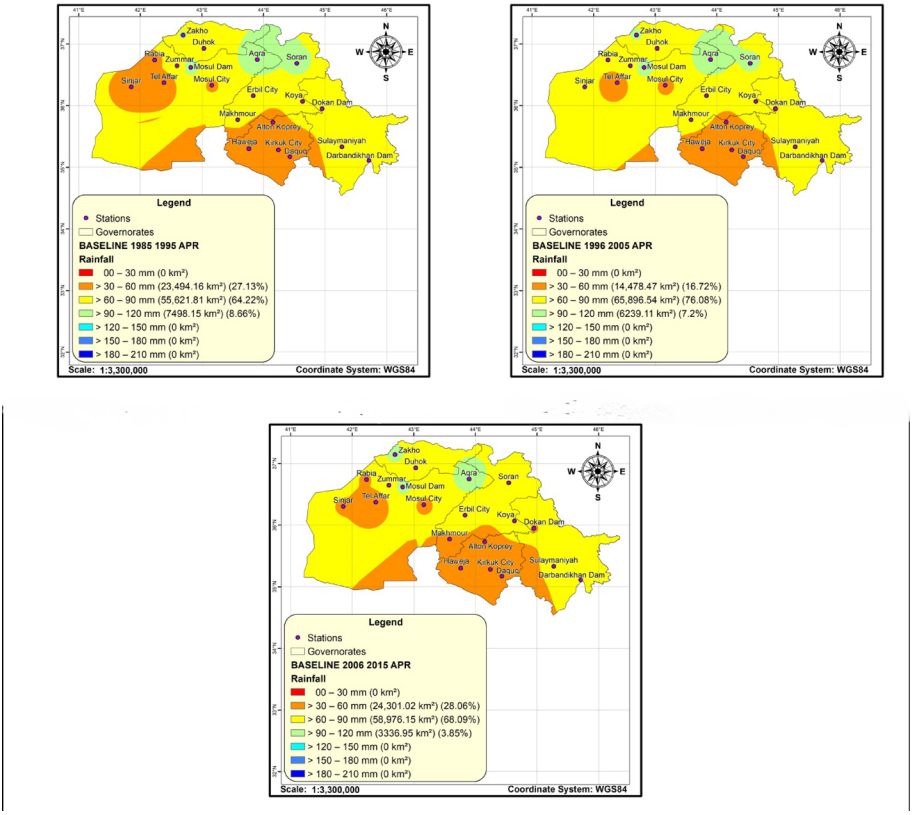

Fig. 18 Results for precipitation in April for baseline period (1985-2015)

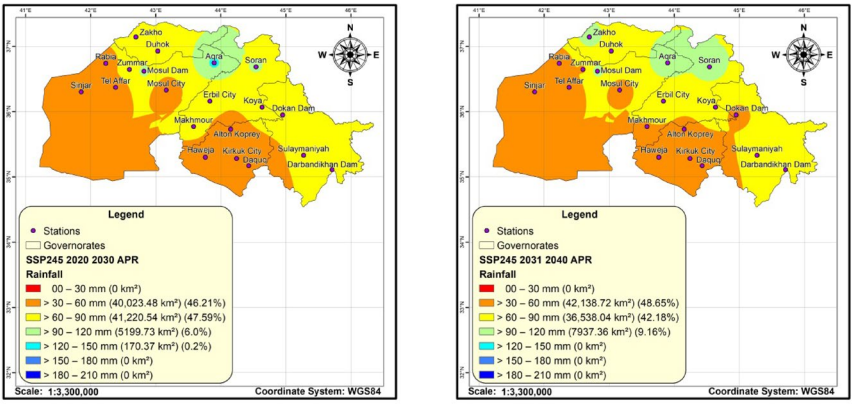

Fig. 19 Results for precipitation in April under SSP245 (2021–2040)

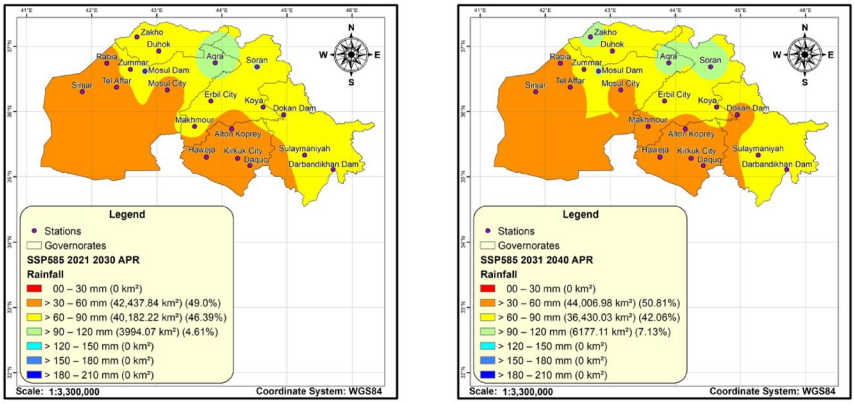

Fig. 20 Results for precipitation in April under SSP585 (2021–2040)

tainous areas such as Aqra, Soran, Zakho, and Mosul Dam. No rainfall exceeding 120 mm was recorded during this interval. In the second interval (1996–2005), the 60–90 mm class accounted for 76.08% of the region's precipitation, while the 30–60 mm class accounted for 16.72%. The highest class (90–120 mm) had a limited presence (7.2%), mainly in mountainous areas (i.e., the same stations in the 1st interval). In the final interval (2006–2015), the 60–90 mm class declined to 68.09%, while the 30–60 mm class increased significantly to 28.06%, and the 90–120 mm class decreased to 3.85%. This gradual trend indicates a general decline in higher precipitation amounts and (consequently) a relative expansion of semi-arid regions, especially in the central and western parts of the studied region, compared to relative stability in medium precipitation in the northeast, such as Aqra, Zakho, and Mosul Dam.

Projected rainfall data for the SSP245 moderate climate scenario during the period (2021–2040) are shown in Fig. 19. For both intervals, rainfall amounts are projected to show a gradual trend toward declining precipitation rates and the expansion of low-rainfall areas,

especially in the south and east regions. In the first interval (2021–2030), the 60–90 mm class will be the most widespread, covering 47.59% of the total area, followed closely by the 30–60 mm class at 46.21%. Areas that will experience precipitation above 90 mm are expected to account for only 8.0% and are clustered in limited areas in the northeast, such as Mosul Dam, Aqra, and Soran. In the second interval (2031–2040), the area of the 30–60 mm class is likely to increase to 48.65%, while the 60–90 mm class will decline to 42.18%, with a slight increase in the 90–120 mm class to 9.16%. Generally, the figure highlights that future rainfall data is likely to decline relative to the 3rd interval of the reference period, and the 2nd interval will have a greater influence than the 1st .

Under the extreme climate change scenario SSP585 (Fig. 20), which assumes continued high emissions and ineffective climate policies, rainfall maps for April during the period (2021–2040) are anticipated to show a more pronounced deterioration in the spatial and temporal distribution of precipitation compared to the moderate scenario. In the first interval (2021–2030), the 30–60 mm class will account for 49.0% of the region, likely distributed in the south and southwest, followed by the 60–90 mm class at 46.39%, anticipated to be located in the north and northeast. The percentage of areas receiving precipitation between 90 and 120 mm will not exceed 4.61% and will likely be concentrated in limited areas in the northeast, at the Mosul Dam and Aqra Stations. In the second interval (2031–2040), the predominance of the 30–60 mm class is projected to increase to 50.81%, likely distributed in the south and southwest areas, while the 60–90 mm class will decline to 42.06%, likely distributed in the south and southwest areas. Meanwhile, the 90–120 mm class will see a slight increase to 7.13%, which may be attributed to the local effects of the high geography at Mosul Dam, Zakho, Aqra, and Soran Stations. Totally, the figure shows that the effect of climate change on future rainfall data is similar to that of the 1st and 2nd intervals under SSP245. The 2nd interval (SSP585) differs from the others in terms of expected future rainfall reductions. It is the most impactful interval, followed by the 2nd (SSP245), 1st (SSP585), and 1st interval (SSP245).

Maps prepared for the observational and predicted periods under two climate scenarios to analyse spatial-temporal rainfall variations during May are presented in Figs. 21, 22 and 23. During the reference period (1985–2015), divided into three consecutive time intervals, the rainfall maps showed clear variation in both spatial and temporal distributions (Fig. 21). The figure reveals a dramatic decline in rainfall amounts compared with the baseline period in all previous months. Additionally, the 0–30 mm class was dominant; the 30–60 mm class was observed in limited areas in the north. In the first interval (1985–1995), the rainfall class (0–30 mm) covered approximately 74.89% of the total area of the study area (64,861.83 km²), while the higher class (30–60 mm) covered only 25.11% (21,752.29 km²). No rainfall exceeding 60 mm was recorded during this interval, indicating a relatively dry month. The highest rainfall was concentrated in the north and west, including Zakho, Duhok, Sinjar, Soran, and parts of Mosul. During the second interval (1996–2005), the extent of drought increased, with the percentage of areas falling into the 0–30 mm class increasing to 89.01% (77,093.44 km²), while the 30–60 mm class shrank to only 10.99% (9,520.68 km²). This class appeared in limited areas in the north of the region, such as Duhok, Zakho, and Soran. This change indicates an apparent worsening of rainfall scarcity compared to the previous interval. During the third interval (2006–2015), this trend continued, with the 0–30 mm class occupying 86.87% of the area (75,245.79 km²), while the 30–60 mm class expanded relatively to 13.13% (11,368.33 km²). The areas with the highest relative rainfall

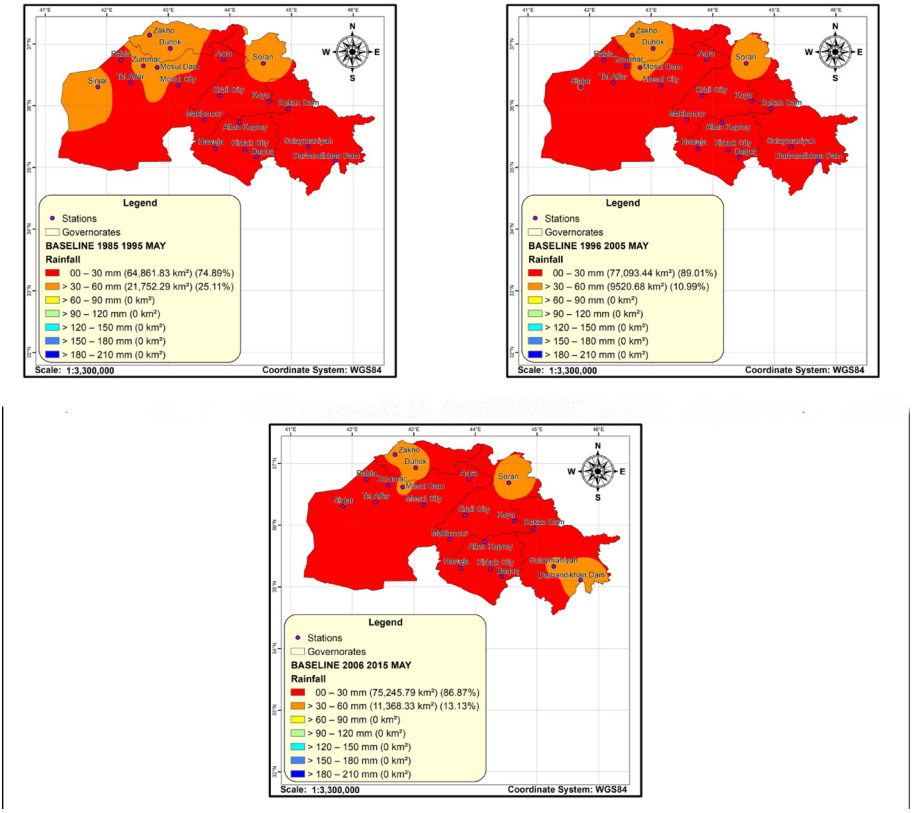

Fig. 21 Results for precipitation in May for baseline period (1985-2015)

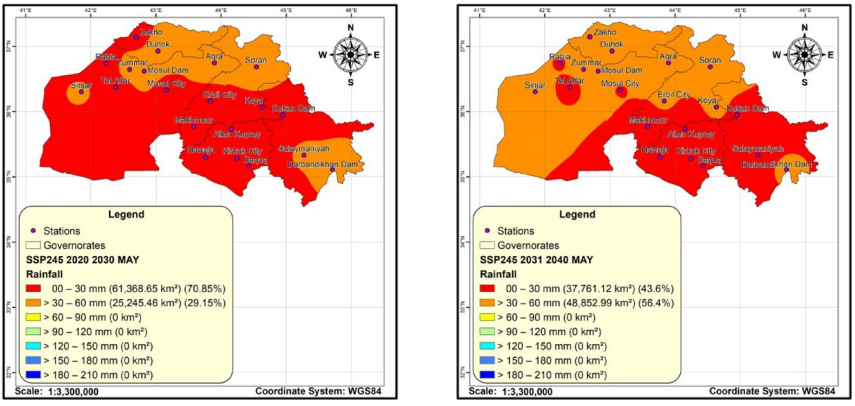

Fig. 22 Results for precipitation in May under SSP245 (2021–2040)

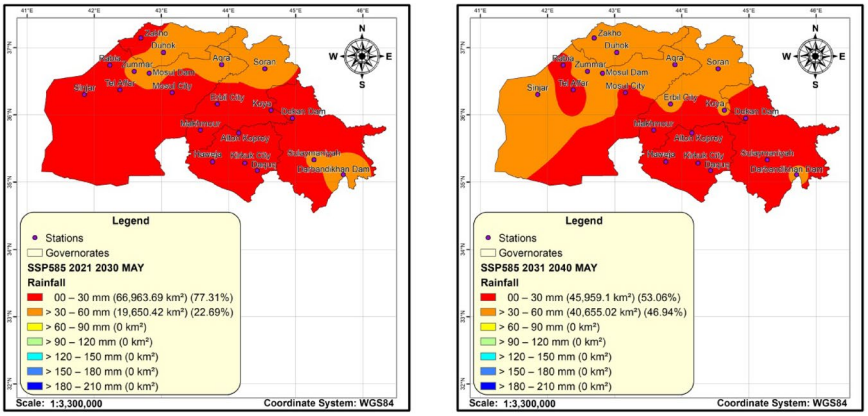

Fig. 23 Results for precipitation in May under SSP585 (2021–2040)

were concentrated in the north, including Zakho, Duhok, Mosul Dam, and Soran, as well as in the southeast, including the Darbandikhan Dam and the Sulaymaniyah City area. Despite this slight improvement in class 2 distribution, the lack of rainfall exceeding 60 mm across all three intervals confirms the continuation of the dry pattern in May. Overall, these maps highlight a clear climatic trend toward declining rainfall rates during May, with a significant expansion in the lower categories and a complete absence of the medium and high classes, which may reflect the impact of climate change in the studied region.

The future rainfall map for May under the SSP245 scenario will indicate a marked variation in the spatial and temporal distribution of rainfall, with lower classes remaining dominant throughout both intervals, reflecting the continued impact of relative aridity in most parts of the study area (Fig. 22). However, maps under SSP245 are likely to have greater 30–60 mm class than maps of baseline period. During the first interval (2021–2030), the 0–30 mm class will probably dominated the majority of the area, accounting for 70.85% (61,368.65 km²), while the 30–60 mm class is expected to accounted for 29.15% (25,245.46 km²), concentrated in northern and eastern areas such as Zakho, Duhok, Soran, and Darbandikhan Dam, with limited occurrence around Sinjar. Medium and high rainfall classes (>60 mm) were completely absent. In the second interval (2031–2040), the percentage of the lowest class is projected to decrease to 43.6% (37,761.12 km²), while the 30–60 mm class is expected to expand significantly, covering 56.4% of the area (48,852.99 km²). This change reflects a relative increase in rainfall abundance compared to the previous interval, especially in the north and northwest, and the 2nd interval will likely witness rainfall amounts greater than in the 1st. However, rainfall remains confined to the low and medium classes, with no precipitation exceeding 60 mm.

In Fig. 23, future May precipitation maps will show a general drying trend and an increase in areas falling into the lower precipitation classes under the intense warming and land-use of SSP585, with small shifts in spatial distribution across the various intervals. The 1st interval of both SSPs is likely to exhibit the same rainfall-class pattern. It is expected that the same will occur for the 2nd interval for both SSPs. However, the 2nd interval (SSP245) is projected to receive the highest rainfall amounts, followed by the 2nd (SSP585), the 1st (SSP245), and the 1st (SSP585). No rainfall class is likely to exceed 60 mm during

the scenario. Drought's dominance in the climate landscape is evident in the first interval (2021–2030), with the 0–30 mm class is anticipated to account for 77.31% of the total area (66,963.69 km²). Meanwhile, the 30–60 mm class is expected to be observed in some northern and eastern regions, including Aqra, Duhok, Soran, and Darbandikhan, accounting for 22.69% (19,650.42 km²). Medium- and high-rainfall classes will probably be completely absent. In the second interval (2031–2040), the situation focused on the 0–30 mm and 30–60 mm classes, which are somewhat expected to improve, and the 0–30 mm class will reduce to 53.06% (45,959.1 km²), and the 30–60 mm class will increase to 46.94% (40,655.02 km²). An improvement in relative rainfall concentration in this region is evident, particularly in the northwest, but it is not sustained.

4 Discussion

According to this research's findings, the LARS-WG model has sufficient capacity to simulate monthly rainfall trends in the study area during the baseline period (1985–2015), as demonstrated by the statistical performance shown in Table S4. The RMSE and MAE values were acceptable, indicating that the model adequately captured the overall variability of monthly rainfall, and the low MBE value indicated minimal bias in the generated series. The correlation coefficient R indicated a moderately positive association between the observed and simulated data, and the Brier Score indicated a good probability accuracy of the methodology in modelling the rainfall events- an indicator lacking use in past Iraqi research, and therefore, reinforced the methodological side of the research.

In the future, the outcomes for the 2031 to 2040 period under the SSP245 and SSP585 scenarios indicate that future rainfall patterns will not change with seasons, but will exhibit distinct monthly variations. Fig. S2 represents a small positive change over the highest emission scenario (SSP585) in the rainfall of December-March, which is also in line with what is reported in the literature of the region, e.g. Munawar et al. (2022) in Pakistan, Siddig et al. (2020) in Sudan, and Ghasemi and Dariane (2026) in Iran, stating that more rainfall in winter months is possible due to increased atmospheric instability.

The climate maps produced in this study showed that topographic elevation and precipitation pattern were significantly correlated. The highest precipitation was observed in the north and northeast of the study area, particularly in the mountainous areas around the Zakho, Duhok, and Soran Stations. This is because the elevated terrain lifts moist air, increasing the likelihood of condensation and precipitation. This geographical distribution aligns with other regional studies examining the effect of topography on rainfall distribution in Iraq and the surrounding areas, including Kavwenje et al. (2021) and Sheikhbabaei et al. (2022).

The 10-year time intervals can be regarded as a substantial methodological contribution to this study because they enabled the detection of the slightest changes in monthly precipitation trends, which are unlikely to be observed in seasonal and long-term analyses. The implications of this segmentation were that the distribution of future rainfall showed consistency in the timing of the highest rainfall in the past and future, but also an evident monthly variation that differs in intensity and direction between the SSP245 and SSP585 scenarios. This trend is in line with the results from previous regional studies i.e. Afshar et al. (2020) (Turkey), Usta et al. (2021)(Iran), Mohammed and Fallah (2019)(Syria), and

Kosasaeng (2025), who also revealed that climate change causes fluctuations in the amount of precipitation in a month without obvious signs of a change in the time of the most significant rainfall events. These findings highlight the significance of the monthly analysis used in this research, especially in rainfed agricultural regions of northern Iraq, which depend not only on rainfall amounts but also on its monthly distribution.

As the comparison of the two climate scenarios revealed, the high-emission scenario (SSP585) shows more pronounced future precipitation changes, i.e., rainfall will be considerably reduced in most study areas. However, the transition in the SSP245 scenario appears less radical, and the north of the country will likely maintain a relative balance of rainfall. Those trends indicate a high probability of rising water stress in the southern and western parts of the study area, as rainfall is expected to decrease in the coming decades. This may have a detrimental effect on the water and farm security in rain-fed set-ups. Our results are in line with other studies, such as Abdulhussein et al. (2024), who found that, as GHG concentrations persist, precipitation decreases further in arid and semi-arid areas. The apparent disparities between the two situations in this experiment suggest some uncertainty in future rainfall predictions, which is common in CMIP6 models in dry and semi-dry regions, as precipitation is highly variable and sensitive to local weather patterns.

This study revealed that rainfed agricultural lands in northern Iraq are highly sensitive to even slight monthly rainfall changes, as this region relies solely on rainfall with no irrigation systems. This tendency is consistent with the results of several reviewed regional studies (Turkey, Iran, Syria), which showed that a shift in the timing of peak rainfall is not always caused by climate change. However, it does cause significant monthly changes in rainfall rates, which directly affect planting dates and crop yields in arid and semi-arid regions.

At the regional level, this study has ample agreement with the findings of Mohammed and Fallah (2019), Afshar et al. (2020), Usta et al. (2021), Tarawneh and Chowdhury (2018), Kavwenje et al. (2021), Avazpour et al. (2025), and Khan and Naeem (2023) mainly concerning the fact that: A high degree of uncertainty in rainfall forecasts; some increase in rainfall in some months and decrease in others; and the arid and semi-arid areas faced oscillatory influence due to climate change instead of linear trend. The fact that the results of this work are similar to those of the regional studies further strengthens our work's credibility. It demonstrates that future precipitation changes in northern Iraq are not unique but part of an overall trend that extends across vast areas of West Asia.

These results are important as they have taken into account agriculture, food security, and water resource management. The monthly behaviour suggests a strong need to develop agricultural early warning systems from monthly time-series data rather than from annual indicators. Analyses of these kinds of decisions may be extended to agricultural risk assessment in northern Iraq, thereby suggesting that such data could be used for broader consideration in the agriculture sector.

5 Limitations

Generally, the outcomes of this research provide insight into future climate conditions and freshwater availability in Northern Iraq. However, this study has multiple potential limitations and sources of uncertainty, but those could be valuable in future investigations. The climate projections' uncertainties in this work can be broadly divided into five groups:

- Observation data: our research used CHRIPS data because continuous data were unavailable during the baseline period. The quality of observations determines the quality of the projected data with less bias (Wu et al. 2022). Using observations from additional sources could make our results more robust, so it's absolutely possible for future enhancements.
- Projection model: there may be uncertainty in the generation of synthetic climate data by the LARS-WG model due to limited historical climate data used for LARS-WG calibration, potentially leading to the omission of extreme weather events (Liu et al. 2023). It is recommended to apply other statistical downscaling methods in the future.
- GHG emission scenarios: 2 scenarios (SSP245 and SSP585) were applied in this research. Projections are significantly affected by uncertainty about future emission pathways, such as those outlined in the Shared Socioeconomic Pathways (SSPs) and Representative Concentration Pathways (RCPs) (Abdeyazdan et al. 2026). As mentioned by Tibangayuka et al. (2022), involving extra emission scenarios in hydrological research is significant for better understanding the related uncertainties. Consequently, it is recommended to apply further emission scenarios to generalise the investigation's outcomes.
- GCMs: the research has been conducted using downscaled and bias-corrected CMIP6 model results, which, although improved over earlier versions, inherently have biases and uncertainties due to differences in emission scenarios, parameterisations, and model physics. The multi-model ensemble average has been used to reduce GCM uncertainties, as in earlier investigations (Singh et al. 2026). However, uncertainties could arise from the GCMs used in the ensembles not being sufficiently robust (Liu et al. 2023). The outcomes of this research are based on only 6 GCMs. Hence, it is recommended to incorporate further GCMs, if available, to generalise the research outcomes.
- Internal variability: despite using the same model under the same external conditions, inherent fluctuations arise from the chaotic nature of the climate system (Abdeyazdan et al. 2026).

6 Conclusion

This study set out to examine the extent to which climate change impacts rainfall spatial-temporal patterns by comparing the baseline period (1985–2015) with the future period (2021–2040) across 5 intervals, each approximately 1 decade. The LARS-WG (8) was integrated with six GCMs under the CMIP6 and two GHG scenarios (SSP245 and SSP585) to project rainfall data, and ArcGIS and IWD techniques were employed to represent the data spatially across 20 stations (5 governorates). Based on the research examining LARS-WG's capacity to simulate rainfall data during the baseline period, the model emerged as a reliable predictor and can be used to generate future data across 6 statistical criteria and a graphical

test (Sect. 3.1). For instance, in Daquq Station, the rainfall data was well simulated with a *P* value ranging from very good to perfect, a Brier Score value (0.070), and MBE (− 0.52).

After that, daily rainfall data were projected for all stations, and the GCM ensemble mean was computed. This method, stated by Tibangayuka et al. (2022), offers reliable evaluations because averaging GCM results smooths climatic variability. The rainfall data were divided into 7 classes from 0 to 210 mm, each with a range of about 30 mm for historical and future data from November to May. One of the more significant findings to emerge from this study is that future intervals under both scenarios are likely to receive less rainfall than the 3rd interval of the historical period for November, January, February, and April. In contrast, December and May are expected to receive more rainfall than the 3rd interval of the historical period. The research has also shown that the highest rainfall class (180–210 mm) at Aqra Station in January covered 0.16% of the total area during 19,962,005. It is anticipated to appear at the same station and month, covering 0.23% and 0.08% under SSP245 (2021–2030) and SSP585 (2021–2030), respectively. In May, rainfall classes have been classified into 0–30 mm and 30–60 mm in the past, and they are projected to remain the same in the future under both scenarios. However, the 30–60 mm class is likely to increase from 13.13% (2006–2015) to 22.69% (SSP585, 2021–2030) and to 56.4% (SSP245, 2031–2040).

All nominated months are forecast to exhibit spatial shifts across rainfall classes under both scenarios. For example, during March, rainfall of 150–180 mm class shifted from Mosul Dam, covering 161.66 km2 (1995–2006), to likely Dokan Dam, covering 204.89 km^2 (SSP585, 2031–2040). These spatial shifts are anticipated to happen with no clear temporal shifts in rainfall timing. Therefore, with this choice, we can probably expect no change in the seasons, meaning that farming practices, ecosystems, and human activities will also remain unchanged.

These results underscore the need for rapid, effective responses from Iraqi authorities. This response must include improving water management strategies, developing smart irrigation technologies, and enhancing water-harvesting strategies by maintaining existing dams and constructing new ones.

Supplementary Information The online version contains supplementary material available at https://doi.org/10.1007/s11069-026-08271-x.

Author contributions Tuqa Khalid Abed: Formal analysis, Investigation, Methodology, Validation, Writing - original draft, Writing - review & editing. Salah L. Zubaidi: Methodology, Conceptualization, Project administration, Supervision, Software, Writing - review & editing. Yousif Almamalachy: Data curation, Investigation, Software, Resources, Visualization, Mustafa Al-Mukhtar: Methodology, Writing - review & editing. Mawada Abdellatif: Methodology, Software, Writing - review & editing. Sura Mohammed Abdulsahib: Data curation, Investigation, Software, Visualization. Hatem Hameed Hussein: Methodology, Data curation, Investigation, Software.

Funding No funding was received for this research.

Declarations

Conflict of interest The authors declare that they have no competing interests.

References

Abdeyazdan A, Ahmadi A, Torabi Haghighi A (2026) Projection of non-stationary compound droughts considering internal variability of a climate model over Iran. Hydrol Sci J 71(2):325–343. https://doi.org/10.1080/02626667.2025.2594621

Abdulhussein HK, Al-Lami AM, Hashim BM (2024) Projection of precipitation under RCP4.5 and RCP 8.5 in central and southern regions of Iraq. J Agrometeorology 26(3):295–299. https://doi.org/10.54386/jam.v26i3.2575

Abdulsahib SM, Zubaidi SL, Almamalachy Y, Dulaimi A (2024) Temperature and precipitation change assessment in the North of Iraq using LARS-WG and CMIP6 models. Water. https://doi.org/10.3390/w16192869

Abedi-Koupai J, -M Dorafshan M, Javadi A, Ostad-Ali-Askari K (2022) Estimating potential reference evapotranspiration using time series models (case study: synoptic station of Tabriz in northwestern Iran). Appl Water Sci 12(9):1–8. https://doi.org/10.1007/s13201-022-01736-x

Adamo N, Al-Ansari N, Sissakian VK, Knutsson S, Laue J (2018) Climate change: consequences on Iraq's environment. J Earth Sci Geotech Eng 8(3)

Afshar MH, Şorman AÜ, Tosunoğlu F, Bulut B, Yilmaz MT, Danandeh Mehr A (2020) Climate change impact assessment on mild and extreme drought events using copulas over Ankara, Turkey. Theoret Appl Climatol 141(3–4):1045–1055. https://doi.org/10.1007/s00704-020-03257-6

Ahmad HQ, Kamaruddin SA, Harun SB, Al-Ansari N, Shahid S, Jasim RM (2021) Assessment of spatiotemporal variability of meteorological droughts in Northern Iraq using satellite rainfall data. KSCE J Civ Eng 25(11):4481–4493. https://doi.org/10.1007/s12205-021-2046-x

Al-Hasani B, Abdellatif M, Carnacina I, Harris C, Al-Quraishi A, Maaroof BF, Zubaidi SL (2023) Integrated geospatial approach for adaptive rainwater harvesting site selection under the impact of climate change. Stoch Env Res Risk Assess 38(3):1009–1033. https://doi.org/10.1007/s00477-023-02611-0

Alam MS, Barbour SL, Elshorbagy A, Huang M (2018) The impact of climate change on the water balance of oil sands reclamation covers and natural soil profiles. J Hydrometeorol 19(11):1731–1752. https://doi.org/10.1175/jhm-d-17-0230.1

Alam MS, Barbour SL, Huang M, Li Y (2020) Using statistical and dynamical downscaling to assess climate change impacts on mine reclamation cover water balances. Mine Water Environ 39(4):699–715. https://doi.org/10.1007/s10230-020-00695-6

Alasow AA, Hamed MM, Shahid S (2024) Spatiotemporal variability of drought and affected croplands in the horn of Africa. Stoch Env Res Risk Assess 38(1):281–296

Avazpour F, Hadian MR, Talebi A, Torabi Haghighi A (2025) Impact of climate change on river flow, using a hybrid model of LARS_WG and LSTM: a case study in the Kashkan Basin. Results Eng. https://doi.org/10.1016/j.rineng.2025.104956

Awchi TA, Kalyana MM (2017) Meteorological drought analysis in northern Iraq using SPI and GIS. Sustain Water Resour Manage 3(4):451–463. https://doi.org/10.1007/s40899-017-0111-x

Azad N, Ahmadi A (2024) Assessment of CMIP6 models and multi-model averaging for temperature and precipitation over Iran. Sci Rep 14(1):24165. https://doi.org/10.1038/s41598-024-74789-4

Bessah E, Raji AO, Taiwo OJ, Agodzo SK, Ololade OO (2020) The impact of varying spatial resolution of climate models on future rainfall simulations in the Pra River Basin (Ghana). J Water Clim Change 11(4):1263–1283. https://doi.org/10.2166/wcc.2019.258

Bilbao-Barrenetxea N, Martínez-España R, Jimeno-Sáez P, Faria SH, Senent-Aparicio J (2024) Multi-model ensemble machine learning approaches to project climatic scenarios in a River Basin in the Pyrenees. Earth Syst Environ 8(4):1159–1177. https://doi.org/10.1007/s41748-024-00408-x

Birara H, Pandey R, Mishra SK (2020) Projections of future rainfall and temperature using statistical downscaling techniques in Tana Basin, Ethiopia. Sustain Water Resour Manag. https://doi.org/10.1007/s40899-020-00436-1

Chen C, Gan R, Feng D, Yang F, Zuo Q (2022) Quantifying the contribution of SWAT modeling and CMIP6 inputting to streamflow prediction uncertainty under climate change. J Clean Prod 364:132675. https://doi.org/10.1016/j.jclepro.2022.132675

Cruz–González1 A (2025) Climate change projections in temperature and precipitation using cmip6 in Central Mexico. J Theoretical and Applied Climatology Quevedo–Nolasco6 A. https://doi.org/10.1007/s00704-024-05345-3

Dheyaa MA, Al-Mukhtar MM, Shemal K (2024) Analyzing the future climate change impacts on meteorological parameters using the LARS-WG model. Civil Eng J 10(11):3754–3778. https://doi.org/10.28991/cej-2024-010-11-019

Ewaid SH, Abed SA, Al-Ansari N (2019) Water footprint of wheat in Iraq. J Water 11(3):535. https://doi.org/10.3390/w11030535

Ewaid SH, Abed SA, Al-Ansari N (2020) Assessment of main cereal crop trade impacts on water and land security in Iraq. Agronomy. https://doi.org/10.3390/agronomy10010098

Ghasemi M, Dariane AB (2026) Assessing climate change impacts on streamflow under uncertainty: multimetric ensemble GCM selection using TOPSIS and social choice. Results Eng. https://doi.org/10.1016/j.rineng.2026.109347

Gitau MW, Mehan S, Guo T (2018) Weather generator effectiveness in capturing climate extremes. Environ Processes 5(S1):153–165. https://doi.org/10.1007/s40710-018-0291-x

Guo X, Huang J, Luo Y, Zhao Z, Xu Y (2017) Projection of heat waves over China for eight different global warming targets using 12 CMIP5 models. Theoret Appl Climatol 128(3–4):507–522. https://doi.org/10.1007/s00704-015-1718-1

Hamed MM, Nashwan MS, Shiru MS, Shahid S (2022) Comparison between CMIP5 and CMIP6 models over MENA region using historical simulations and future projections. Sustainability. https://doi.org/10.3390/su141610375

Hassan WH, Hashim FSJSAS (2020) The effect of climate change on the maximum temperature in Southwest Iraq using HadCM3 and CanESM2 modelling. 2(9):1494

Hassan WH, Nile BK, Kadhim ZK, Mahdi K, Riksen M, Thiab RF (2023) Trends, forecasting and adaptation strategies of climate change in the middle and west regions of Iraq. SN Appl Sci 5(12):1–20. https://doi.org/10.1007/s42452-023-05544-z

Hassan WH, Mahdi K, Kadhim ZK (2025a) GIS-based multi-criteria decision making for identifying rainwater harvesting sites. Appl Water Sci 15(3):1–24. https://doi.org/10.1007/s13201-025-02378-5

Hassan WH, Nile BK, Kadhim ZK, Thiab RF (2025b) Evaluation of the efficiency of Kerbala's rainwater drainage system in dealing with extreme rainfall events during the next decade. In: 7th International Conference on Engineering Sciences – Ices23, AIP, Karbala, Iraq, pp. 1–13

Hernanz A, García-Valero JA, Domínguez M, Ramos-Calzado P, Pastor-Saavedra MA, Rodríguez-Camino E (2021) Evaluation of statistical downscaling methods for climate change projections over Spain: present conditions with perfect predictors. Int J Climatol 42(2):762–776. https://doi.org/10.1002/joc.7271

Hinge G, Surampalli RY, Goyal MK (2018) Prediction of soil organic carbon stock using digital mapping approach in humid India. Environ Earth Sci. https://doi.org/10.1007/s12665-018-7374-x

Jalal HK, Hassan WH, Nile BK (2025) Projected the impacts of climate change on the unconfined Aquifer region, Western Iraq, using LARS-WG and CMIP6 scenarios. Water Conserv Sci Eng 10(2):1–23. https://doi.org/10.1007/s41101-025-00410-y

Jasim AI, Awchi TA (2020) Regional meteorological drought assessment in Iraq. Arab J Geosci. https://doi.org/10.1007/s12517-020-5234-y

Kavwenje S, Zhao L, Chen L, Chaima E (2021) Projected temperature and precipitation changes using the LARS-WG statistical downscaling model in the Shire River Basin, Malawi. Int J Climatol 42(1):400–415. https://doi.org/10.1002/joc.7250

Khairan HE, Zubaidi SL, Raza SF, Hameed M, Al-Ansari N, Ridha HM (2023) Examination of single- and hybrid-based metaheuristic algorithms in ANN reference evapotranspiration estimating. J Sustain 15(19):14222. https://doi.org/10.3390/su151914222

Khalaf RM, Hussein HH, Hassan WH, Mohammed ZM, Nile BK (2022) Projections of precipitation and temperature in Southern Iraq using a LARS-WG Stochastic weather generator. Phys Chem Earth Parts A/B/C 128:1–13. https://doi.org/10.1016/j.pce.2022.103224

Khan SF, Naeem UA (2023) Future climate projections using the LARS-WG6 downscaling model over Upper Indus Basin, Pakistan. Environ Monit Assess 195(7):810. https://doi.org/10.1007/s10661-023-11419-y

Kosasaeng S (2025) Hybrid modeling for future inflow prediction of huai luang reservoir under climate change. Int J GEOMATE. https://doi.org/10.21660/2025.132.4978

Lee CY, Camargo SJ, Sobel AH, Tippett MKJJC (2020) Statistical–dynamical downscaling projections of tropical cyclone activity in a warming climate. Two Diverging Genesis Scenarios 33:4815–4834

Lee H, Calvin K, Dasgupta D, Krinmer G, Mukherji A, Thorne P, Trisos C, Romero J, Aldunce P, Barret K (2023) Synthesis report of the IPCC Sixth Assessment Report (AR6), Longer report. IPCC

Liu Y, Chen X, Gao H, Sha J, Li X (2023) The impacts of climate changes on watershed streamflow and total dissolved nitrogen in Danjiang Watershed, China. J Water Clim Change 14(1):104–122. https://doi.org/10.2166/wcc.2022.213

Marcellin MC, Pavur G, Loose DC, Cardenas JJ, Denehy D, Almashhadani M, Waheed SQ, Trump BD, Polmateer TL, Linkov I, Lakshmi V, Lambert JH (2024) Systems analysis for energy assets of Iraq influenced by water scarcity. Environ Syst Decisions 44(2):259–279. https://doi.org/10.1007/s10669-024-09967-w

Merabti A, Martins DS, Meddi M, Pereira LSJW (2018) Spatial and time variability of drought based on SPI and RDI with various time scales. Water Resour Manage 32:1087–1100

Miralha L, Muenich RL, Scavia D, Wells K, Steiner AL, Kalcic M, Apostel A, Basile S, Kirchhoff CJ (2021) Bias correction of climate model outputs influences watershed model nutrient load predictions. Sci Total Environ 759:143039. https://doi.org/10.1016/j.scitotenv.2020.143039

Modi PA, Fuka DR, Easton ZM (2021) Impacts of climate change on terrestrial hydrological components and crop water use in the Chesapeake Bay watershed. J Hydrol Reg Stud. https://doi.org/10.1016/j.ejrh.2021.100830

Mohammed SA, Fallah RQ (2019) Climate change indicators in Alsheikh-Badr Basin (Syria). Geogr Environ Sustain 12(2):87–96. https://doi.org/10.24057/2071-9388-2018-63

Mohammed ZM, Hassan WH (2022) Climate change and the projection of future temperature and precipitation in southern Iraq using a LARS-WG model. Model Earth Syst Environ. https://doi.org/10.1007/s40808-022-01358-x

Mohammed R, Scholz M (2019) Climate variability impact on the spatiotemporal characteristics of drought and Aridityin arid and semi-arid regions. Water Resour Manage 33(15):5015–5033. https://doi.org/10.1007/s11269-019-02397-3

Mueller A, Detges A, Pohl B, Reuter MH, Rochowski L, Volkholz J, Woertz E (2021) Climate change, water and future cooperation and development in the Euphrates-Tigris basin

Muhaisen NK, Khayyun TS, Al Mukhtar M, Hassan WH (2024) Forecasting changes in precipitation and temperatures of a regional watershed in Northern Iraq using LARS-WG model. Open Eng. https://doi.org/10.1515/eng-2022-0567

Muhire I, Tesfamichael S, Ahmed F, Minani E (2018) Climatology a Spatio-temporal trend analysis of projected precipitation data over Rwanda. Theoret Appl Climatol 131:671–680

Munawar S, Rahman G, Moazzam MFU, Miandad M, Ullah K, Al-Ansari N, Linh NTT (2022) Future climate projections using SDSM and LARS-WG downscaling methods for CMIP5 GCMs over the transboundary Jhelum River Basin of the Himalayas Region. Atmosphere https://doi.org/10.3390/atmos13060898

Musayev S, Burgess E, Mellor J (2018) A global performance assessment of rainwater harvesting under climate change. Resour Conserv Recycl 132:62–70. https://doi.org/10.1016/j.resconrec.2018.01.023

Namdar R, Karami E, Keshavarz M (2021) Climate change and vulnerability: the case of MENA countries. ISPRS Int J Geo-Inf 10(11):794

Nguyen PL, Alexander LV, Thatcher MJ, Truong SCH, Isphording RN, McGregor JL (2024) Selecting CMIP6 global climate models (GCMs) for coordinated regional climate downscaling experiment (CORDEX) dynamical downscaling over Southeast Asia using a standardised benchmarking framework. Geosci Model Dev 17(19):7285–7315. https://doi.org/10.5194/gmd-17-7285-2024

Nile BK, Hassan WH, Alshama GA, Sciences A (2019) Analysis of the effect of climate change on rainfall intensity and expected flooding by using ANN and SWMM programs. ARPN J Eng 14:974–984

Ostad-Ali-Askar K, Su R, Liu L (2018) Water resources and climate change. J Water Clim Change 9(2):239–239. https://doi.org/10.2166/wcc.2018.999

Ostad-Ali-Askari K, Ghorbanizadeh Kharazi H, Shayannejad M, Zareian MJ (2019) Effect of management strategies on reducing negative impacts of climate change on water resources of the Isfahan–Borkhar aquifer using MODFLOW. River Res Appl 35(6):611–631. https://doi.org/10.1002/rra.3463

Pereira FC, Gonçalves AM, Costa M (2023) Short-term forecast improvement of maximum temperature by state-space model approach: the study case of the TO CHAIR project. Stoch Env Res Risk Assess 37(1):219–231. https://doi.org/10.1007/s00477-022-02290-3

Price R (2018) In: Report (ed) Environmental risks in Iraq. K. D. H. Institute of Development Studies, Brighton, UK

Rafiei-Sardooi E, Azareh A, Joorabian Shooshtari S, Parteli EJR (2022) Long-term assessment of land-use and climate change on water scarcity in an arid basin in Iran. Ecol Model. https://doi.org/10.1016/j.ecolmodel.2022.109934

Reder A, Fedele G, Manco I, Mercogliano P (2025) Estimating pros and cons of statistical downscaling based on EQM bias adjustment as a complementary method to dynamical downscaling. Sci Rep 15(1):621. https://doi.org/10.1038/s41598-024-84527-5

Sabri NQ, Khayyun TS (2024) Estimation of future climate change in low folded zone, Iraq with the LARS-WG and five GMS models under CMIP5 scenarios. J Ecohumanism. https://doi.org/10.62754/joe.v3i8.4898

Saddique N (2019) Downscaling of CMIP5 models output by using statistical models in a data scarce mountain environment (Mangla Dam Watershed), Northern Pakistan. Asia-Pac J Atmos Sci. https://doi.org/10.1007/s13143-019-00111-2

Saeed FH, Al-Khafaji MS, Al-Faraj FAM (2021) Sensitivity of irrigation water requirement to climate change in arid and semi-arid regions towards sustainable management of water resources. Sustainability. https://doi.org/10.3390/su132413608

Saeed FH, Al-Khafaji MS, Al-Faraj F (2022) Hydrologic response of arid and semi-arid river basins in Iraq under a changing climate. J Water Clim Change 13(3):1225–1240. https://doi.org/10.2166/wcc.2022.418

Sayadi A, Beydokhti NT, Najarchi M, Najafizadeh MM (2019) Investigation into the effects of climatic change on temperature, rainfall, and runoff of the doroudzan catchment, Iran, using the ensemble approach of CMIP3 climate models. Adv Meteorol 2019:1–16. https://doi.org/10.1155/2019/6357912

Senatore A, Fuoco D, Maiolo M, Mendicino G, Smiatek G, Kunstmann H (2022) Evaluating the uncertainty of climate model structure and bias correction on the hydrological impact of projected climate change in a Mediterranean catchment. J Hydrol Reg Stud. https://doi.org/10.1016/j.ejrh.2022.101120

Sha J, Li X, Yang J (2021) Estimation of watershed hydrochemical responses to future climate changes based on CMIP6 scenarios in the Tianhe River (China). Sustainability. https://doi.org/10.3390/su131810102

Sharma A, Sharma D, Panda S, Dubey SK, Pradhan RK (2018) Investigation of temperature and its indices under climate change scenarios over different regions of Rajasthan state in India. Global Planet Change 161:82–96. https://doi.org/10.1016/j.gloplacha.2017.12.008

Shaygan M, Reading LP, Arnold S, Baumgartl T (2018) Modeling the effect of soil physical amendments on reclamation and revegetation success of a saline-sodic soil in a semi-arid environment. Arid Land Res Manage 32(4):379–406. https://doi.org/10.1080/15324982.2018.1510439

Sheikhbabaei A, Hosseini Baghanam A, Zarghami M, Pouri S, Hassanzadeh E (2022) System thinking approach toward reclamation of regional water management under changing climate conditions. Sustainability. https://doi.org/10.3390/su14159411

Siddig K, Stepanyan D, Wiebelt M, Grethe H, Zhu T (2020) Climate change and agriculture in the Sudan: Impact pathways beyond changes in mean rainfall and temperature. Ecol Econ. https://doi.org/10.1016/j.ecolecon.2019.106566

Singh HV, Joshi N, Suryavanshi S (2026) Assessment of drought propagation characteristics in the Betwa river basin under CMIP6 climate projections. Hydrol Sci J 71(3):565–585. https://doi.org/10.1080/02626667.2025.2603421

Song YH, Chung E-S, Shiru MS (2020) Uncertainty analysis of monthly precipitation in GCMs using multiple bias correction methods under different RCPs. Sustainability. https://doi.org/10.3390/su12187508

Talukder A, Shaid S, Hwang S, Alam E, Islam K, Kamruzzaman M (2025) Optimizing the multi-model ensemble of CMIP6 GCMs for climate simulation over Bangladesh. Sci Rep 15(1):11343. https://doi.org/10.1038/s41598-025-96446-0

Tandon A, Awasthi A, Pattnayak KC (2025) Efficacy of machine learning in simulating precipitation and its extremes over the capital cities in North Indian states. Sci Rep 15(1):10345. https://doi.org/10.1038/s41598-024-84360-w

Tarawneh Q, Chowdhury S (2018) Trends of climate change in Saudi Arabia: implications on water resources. Climate. https://doi.org/10.3390/cli6010008

Tibangayuka N, Mulungu DMM, Izdori F (2022) Assessing the potential impacts of climate change on streamflow in the data-scarce Upper Ruvu River watershed, Tanzania. J Water Clim Change 13(9):3496–3513. https://doi.org/10.2166/wcc.2022.208

Trnka M, Balek J, Semenov MA, Semeradova D, Belinova M, Hlavinka P, Olesen JE, Eitzinger J, Schaumberger A, Zahradnicek P, Kopecky D, Zalud Z (2021) Future agroclimatic conditions and implications for European grasslands. Biol Plant 64:865–880. https://doi.org/10.32615/bp.2021.005

Usta DFB, Teymouri M, Chatterjee U, Koley B (2021) Temperature projections over Iran during the twenty-first century using CMIP5 models. Model Earth Syst Environ 8(1):749–760. https://doi.org/10.1007/s40808-021-01115-6

Vallam P, Qin XS (2018) Projecting future precipitation and temperature at sites with diverse climate through multiple statistical downscaling schemes. Theoret Appl Climatol 134(1–2):669–688. https://doi.org/10.1007/s00704-017-2299-y

Vesely FM, Paleari L, Movedi E, Bellocchi G, Confalonieri R (2019) Quantifying uncertainty due to stochastic weather generators in climate change impact studies. Sci Rep 9(1):9258. https://doi.org/10.1038/s41598-019-45745-4

Wu Y, Miao C, Fan X, Gou J, Zhang Q, Zheng H (2022) Quantifying the uncertainty sources of future climate projections and narrowing uncertainties with bias correction techniques. Earth's Future. https://doi.org/10.1029/2022ef002963

Xu L, Wang A (2019) Application of the bias correction and spatial downscaling algorithm on the temperature extremes from CMIP5 multimodel ensembles in China. Earth Space Sci 6(12):2508–2524. https://doi.org/10.1029/2019ea000995

Zubaidi SL, Kumar P, Al-Bugharbee H, Ahmed AN, Ridha HM, Mo KH, El-Shafie A (2023) Developing a hybrid model for accurate short-term water demand prediction under extreme weather conditions: a case study in Melbourne, Australia. Appl Water Sci 13(9):184. https://doi.org/10.1007/s13201-023-01995-2

Authors and Affiliations

Tuqa Khalid Abed[1] · Salah L. Zubaidi[1,2] · Yousif Almamalachy[3] · Mustafa Al-Mukhtar[4] · Mawada Abdellatif[5] · Sura Mohammed Abdulsahib[1] · Hatem Hameed Hussein[6]

✉ Salah L. Zubaidi
salahlafta@uowasit.edu.iq

✉ Mawada Abdellatif
M.E.Abdellatif@ljmu.ac.uk

Tuqa Khalid Abed
Std2023203.T.K@uowasit.edu.iq

Yousif Almamalachy
yogofa@gmail.com

Mustafa Al-Mukhtar
mmalmukhtar@gmail.com

Sura Mohammed Abdulsahib
Std2022203.S.M@uowasit.edu.iq

Hatem Hameed Hussein
p.f.dep@mowr.gov.iq

1 Department of Civil Engineering, Wasit University, Wasit 52001, Iraq

2 College of Engineering, University of Warith Al-Anbiyaa, Karbala 56001, Iraq

3 National Center for Water Resources Management, Ministry of Water Resources, Baghdad, Iraq

4 College of Civil Engineering, University of Technology-Iraq, Baghdad 10066, Iraq

5 School of Engineering and Built Environment, Faculty of Health, Innovation, Technology and Science, Liverpool John Moores University, Liverpool L3 3AF, UK

6 General Director for Planning and Follow up, Ministry for Water Resources, Baghdad, Iraq